1 **Holocene dynamics in the Bering Strait inflow to the Arctic and the Beaufort Gyre**

2 **circulation based on sedimentary records from the Chukchi Sea**

4 Masanobu Yamamoto[1-3*], Seung-Il Nam[4], Leonid Polyak[5], Daisuke Kobayashi[3], Kenta

5 Suzuki[3], Tomohisa Irino[1,3], Koji Shimada[6]

7 *[1]Faculty of Environmental Earth Science, Hokkaido University, Kita-10, Nishi-5,*

8 *Kita-ku, Sapporo 060-0810 Japan*

9 *[2]Global Institution for Collaborative Research and Education, Hokkaido University,*

10 *Kita-10, Nishi-5, Kita-ku, Sapporo 060-0810 Japan*

11 *[3]Gradute School of Environmental Science, Hokkaido University, Kita-10, Nishi-5,*

12 *Kita-ku, Sapporo 060-0810 Japan*

13 *[4]Korea Polar Research Institute, 26 Songdomirae-ro, Yeonsu-gu, Incheon 21990,*

14 *Republic of Korea*

15 *[5]Byrd Polar and Climate Research Center, The Ohio State University, Columbus, OH*

16 *43210USA*

17 *[6]Tokyo University of Marine Science and Technology, 4-5-7, Konan, Minato-ku, Tokyo*

18 *108-8477, Japan.*

19 **Corresponding author. Tel: +81-11-706-2379, Fax: +81-11-706-4867, E-mail address:*

20 *myama@ees.hokudai.ac.jp (M. Yamamoto)*

22 **ABSTRACT**

23 The Beaufort Gyre (BG) and the Bering Strait inflow (BSI) are important elements of

24 the Arctic Ocean circulation system and major controls on the distribution of Arctic sea

ice. We report records of the quartz/feldspar and chlorite/illite ratios in three sediment cores from the northern Chukchi Sea providing insights into the long-term dynamics of the BG circulation and the BSI during the Holocene. The quartz/feldspar ratio, a proxy of the BG strength, gradually decreased during the Holocene, suggesting a long-term decline in the BG strength, consistent with orbitally-controlled decrease in summer insolation. We suppose that the BG rotation weakened as a result of increasing stability of sea-ice cover at the margins of the Canada Basin, driven by decreasing insolation. Millennial to multi-centennial variability in the quartz/feldspar ratio (the BG circulation) is consistent with fluctuations in solar irradiance, suggesting that solar activity affected the BG strength on these timescales. The BSI approximation by the chlorite/illite record, despite a considerable geographic variability, consistently shows intensified flow from the Bering Sea to the Arctic during the middle Holocene, which is attributed primarily to the effect of higher atmospheric pressure over the Aleutian Basin. The intensified BSI was associated with decrease in sea-ice concentrations and increase in marine production, as indicated by biomarker concentrations, suggesting a major influence of the BSI on sea-ice and biological conditions in the Chukchi Sea. Multi-century to millennial fluctuations, presumably controlled by solar activity, were also identified in a proxy-based BSI record characterized with the highest age resolution.

1. Introduction

The Arctic currently faces rapid climate change caused by global warming (e.g., Screen and Simmonds, 2010; Harada, 2016). Changes in the current system of the Arctic Ocean regulate the state of Arctic sea ice and are involved in global processes via

49   ice albedo feedback and the delivery of freshwater to the North Atlantic Ocean (Miller

50   et al., 2010; Screen and Simmonds, 2010). The most significant consequence of this

51   climate change during recent decades is the retreat of summer sea ice in the Pacific

52   sector of the Arctic (e.g., Shimada et al., 2006; Harada et al., 2016, and references

53   therein). Inflow of warm Pacific water through the Bering Strait (hereafter Bering Strait

54   Inflow [BSI]) is suggested to have caused catastrophic changes in sea-ice stability in the

55   western Arctic Ocean (Shimada et al., 2006). Comprehending these changes requires

56   investigation of a longer-term history of circulation in the western Arctic and its

57   relationship to atmospheric forcings. Within this context, the Chukchi Sea is a key

58   region to understand the western Arctic current system as it is located at the crossroads

59   of the BSI and the Beaufort Gyre (BG) circulation in the western Arctic Ocean (Fig. 1)

60   (e.g., Winsor and Chapman, 2004; Weingartner et al., 2005).

61   In this paper we apply mineralogical proxies of the BG and BSI to sediment cores

62   with a century-scale resolution from the northern margin of the Chukchi shelf. The

63   generated record provides new understanding of changes in the BG circulation and BSI

64   strength during most of the Holocene (last ~9 ka). We discuss the possible causes and

65   forcings of the BG and BSI variability, as well as its relationship to sea-ice history and

66   biological production in the western Arctic.

67

68   **2. Background information**

69   *2.1. Oceanographic settings*

70   The wind-driven surface current system of the Arctic Ocean consists of the BG and

71   the Transpolar Drift (TPD) (Proshutinsky and Johnson, 1997; Rigor et al., 2002). This

72   circulation is controlled by the atmospheric system known as the Arctic Oscillation

73   (AO) (Rigor et al., 2002). When the AO is in the positive phase, the BG shrinks back

74   into the Beaufort Sea, the TPD expands to the western Arctic Ocean, and the sea-ice

75   transport from the eastern Arctic to the Atlantic Ocean is intensified. When the AO is in

76   negative phase, the BG expands, the TPD is limited to the eastern Arctic, and sea ice is

77   exported efficiently from the Canada Basin to the eastern Arctic. Thus, sea-ice

78   distribution is closely related to the current system.

79   A dramatic strengthening of the BG circulation occurred during the last two decades

80   (Shimada et al., 2006; Giles et al., 2012). This change was attributed to a recent

81   reduction in sea-ice cover along the margin of the Canada Basin, which caused a more

82   efficient transfer of the wind momentum to the ice and underlying waters in the BG

83   (Shimada et al., 2006). The delayed development of sea ice in winter enhanced the

84   western branch of the Pacific Summer Water across the Chukchi Sea. This anomalous

85   heat flux into the western part of the Canada Basin retarded sea-ice formation during

86   winter, thus, further accelerating overall sea-ice reduction.

87   The BSI, an important carrier of heat and freshwater to the Arctic, transports the

88   Pacific water to and across the Chukchi Sea, interacts with the BG circulation at the

89   Chukchi shelf margin (e.g., Shimada et al., 2006). Mooring data suggest that an increase

90   in the BSI volume by ~50% from 2001 (~0.7 Sv) to 2011 (~1.1 Sv) has driven an

91   according increase in the heat flux from ~3×10^{20} J to ~5×10^{20} J (Woodgate et al.,

92   2012). After passing the Bering Strait the BSI flows in three major branches. One

93   branch, the Alaskan Coastal Current (ACC), runs northeastward along the Alaskan coast

94   as a buoyancy-driven boundary current (Red arrow in Fig. 1; Shimada et al., 2001;

95   Pickart, 2004; Weingartner et al., 2005). The second, central branch follows a seafloor

96   depression between Herald and Hanna Shoals, then turns eastward and merges with the

97 ACC (Yellow arrow in Fig. 1; Winsor and Chapman, 2004; Weingartner et al., 2005).

98 The third branch flows northwestward, especially when easterly winds prevent the ACC

99 (Winsor and Chapman, 2004). This branch may then turn eastward along the shelf break

100 (Blue arrow in Fig. 1; Pickart et al., 2010).

101   The BSI is driven by a northward dip in sea level between the North Pacific and the

102 Arctic Ocean (Shtokman, 1957; Coachman and Aagaard, 1966). There has been a

103 long-standing debate, whether this dipping is primarily controlled by steric difference

104 (Stigebrandt, 1984) or from wind-driven circulations (Gudkovitch, 1962). Stigebrandt

105 (1984) assumed that the salinity difference between the Pacific and Atlantic Oceans

106 causes the steric height difference between the Bering Sea and the Arctic Ocean.

107 Aagaard et al. (2006) argued that the local salinity in the northern Bering Sea controlled

108 the BSI, although wind can considerably modify the BSI on a seasonal timescale. De

109 Boer and Nof (2004) proposed a model that the mean sea level difference along the

110 strait is set up by the global winds, particularly the strong Subantarctic Westerlies.

111   Recently, a conceptual model of the BSI controls has been developed based on a

112 decade of oceanographic observations (Danielson et al., 2014). According to this model,

113 storms centered over the Bering Sea excite continental shelf waves on the eastern

114 Bering shelf that intensify the BSI on synoptic time scales, but the integrated effect of

115 these storms tends to decrease the BSI on annual to decadal time scales. At the same

116 time, an eastward shift and overall strengthening of the Aleutian Low pressure center

117 during the period between 2000–2005 and 2005–2011 increased the sea level pressure

118 in the Aleutian Basin south of the Bering Strait by 5 hPa, in contrast to overall

119 decreased pressure of the Aleutian Low system, thus decreasing the water column

120 density through isopycnal uplift by weaker Ekman suction. This change thereby raised

121   the dynamic sea surface height by 4.2 m along the Bering Strait pressure gradient,

122   resulting in the BSI increase by 4.5 cm/s, or 0.2 Sv (calculated based on the

123   cross-section area of 4.25×10^6 m^2). This increase constitutes about one quarter of the

124   average long-term BSI volume of ~0.8 Sv (Roach et al., 1995). Such a large

125   contribution clearly identifies changes in the Aleutian Low strength and position as a

126   key factor regulating the BSI on inter-annual time scales.

127   The BSI also transports nutrients from the Pacific to the Arctic. A rough estimation

128   suggests that the BSI waters significantly contribute to marine production in the Arctic

129   (Yamamoto-Kawai et al., 2006). High marine production in the Chukchi Sea of up to

130   400 gC m^{-2} y^{-1} in part is thought to reflect the high nutrient fluxes by the BSI (Walsh

131   and Dieterle, 1994; Sakshaug, 2004). A recent enhancement of biological productivity

132   and the biological pump in the Beaufort and Chukchi Seas has been associated with the

133   retreat of sea ice (summarized by Harada et al., 2016). This phenomenon is attributed to

134   an increase of irradiance in the water column (Frey et al., 2011; Lee and Whitledge,

135   2005), wind-induced mixing that replenishes sea surface nutrients (Carmack et al.,

136   2006), and their combination (Nishino et al., 2009). However, the nutrient flux into the

137   Arctic Ocean was not evaluated in this context. The investigation of BSI intensity and

138   marine production during the Holocene will be useful to understand on-going changes

139   in marine production in the Arctic Ocean.

140

141   *2.2. Mineral distribution in the Chukchi Sea sediments*

142   Spatial variation in mineral composition of surficial sediments along the western

143   Arctic margin has been investigated in a number of studies using different

144   methodological approaches but showing an overall consistent picture (e.g., Naidu et al.,

145   1982; Naidu and Mowatt, 1983; Wahsner et al., 1999; Kalinenko, 2001; Viscosi-Shirley

146   et al., 2003; Darby et al., 2011; Kobayashi et al., 2016). A recent study of mineral

147   distribution in sediments from the Chukchi Sea and adjacent areas of the Arctic Ocean

148   and the Bering Sea suggests that the quartz/feldspar (Q/F) ratio is higher on the North

149   American than on the Siberian side of the western Arctic (Fig. 2; Kobayashi et al.,

150   2016). These results are consistent with earlier studies including mineral determinations

151   of shelf sediments and adjacent coasts (Vogt, 1997; Stein, 2008). Darby et al. (2011)

152   show a trend of decreasing Q/F ratio in dirty sea ice from North American margin to the

153   Chukchi Sea and further to the East Siberian Sea. This zonal gradient of the Q/F ratio

154   suggests that quartz-rich but feldspar-poor sediments are derived from the North

155   American margin by the BG circulation, whereas feldspar–rich sediments are delivered

156   to the Chukchi Sea from the Siberian margin by currents along the East Siberian slope

157   (Kobayashi et al., 2016). Thus, this ratio can be used as a provenance index for the BG

158   circulation reflecting changes in its intensity in sediment-core records (Kobayashi et al.,

159   2016).

160   Kaolinite is generally a minor component of clays in the western Arctic but relatively

161   abundant in the Northwind Ridge and Mackenzie Delta areas where the BG circulation

162   exerts an influence (Naidu and Mowatt, 1983; Kobayashi et al., 2016). Kaolinite in the

163   Northwind Ridge originated from ancient rocks exposed on the North Slope and was

164   delivered by water or sea ice via the Beaufort Gyre circulation (Kobayashi et al., 2016).

165   Kobayashi et al. (2016) also indicate that both the (chlorite + kaolinite)/illite and

166   chlorite/illite ratios (CK/I and C/I ratios, respectively) are higher in the Bering Sea and

167   decrease northward throughout the Chukchi Sea, reflecting the diminishing strength of

168   the BSI (Fig. 2). These results are consistent with earlier studies showing that illite is a

169 common clay mineral in Arctic sediments (Kalinenko, 2001; Darby et al., 2011),

170 whereas, chlorite is more abundant in the Bering Sea and the Chukchi shelf areas

171 influenced by the BSI (Naidu and Mowatt, 1983; Kalinenko, 2001; Nwaodua et al.,

172 2014; Kobayashi et al., 2016). Chlorite occurs abundantly near the Bering Sea coasts of

173 Alaska, Canada, and the Aleutian Islands (Griffin and Goldberg, 1963). The

174 chlorite/illite ratio is higher in the bed load of rivers and deltaic sediments from

175 southwestern Alaska than from northern Alaska and East Siberia, reflecting differences

176 in the geology of the drainage basins (Naidu and Mowatt, 1983). Because chlorite

177 grains are more mobile than illite grains under conditions of intense hydrodynamic

178 activity, chlorite grains are transported a long distance from the northern Bering Sea to

179 the Chukchi Sea via the Bering Strait (Kalinenko, 2001). In the surface sediments of the

180 Chukchi Sea, the CK/I ratio shows a good correlation with the C/I ratio, indicating that

181 both ratios can be used as a provenance index for the BSI (Kobayashi et al., 2016).

182 Ortiz et al. (2009) constructed the first chlorite-based Holocene record of the BSI by

183 quantifying the total chlorite plus muscovite abundance based on diffuse spectral

184 reflectance of sediments from a northeastern Chukchi Sea core. The record shows a

185 prominent intensification of the BSI in the middle Holocene. However, a record from

186 just one site is clearly insufficient to characterize sedimentation and circulation history

187 in such a complex area. More records of mineral proxy distribution covering various

188 oceanographic and depositional environments are needed to further our understanding

189 of the evolution of the BSI.

190 The Holocene dynamics of the BG circulation is also poorly understood. A study of

191 sediment core from the northeastern Chukchi slope identified centennial- to

192 millennial-scale variability in the occurrence of Siberian iron oxide grains presumably

193 delivered via the BG (Darby et al., 2012). However, transport of these grains depends

194 not only on the BG, but also on circulation and ice conditions in the Eurasian basin,

195 which complicates the interpretation and necessitates further proxy studies of the BG

196 history.

197

198 **3. Samples and methods**

199 3.1. Coring and sampling

200 This study uses three sediment cores from the northern and northeastern margins of

201 the Chukchi Sea: ARA02B 01A-GC (gravity core; 563 cm long; 73°37.89'N,

202 166°30.98'W), HLY0501-05JPC/TC (jumbo piston core/trigger; 1648 cm long,

203 72°41.68'N, 157°31.20'W) and HLY0501-06JPC (1554 cm long; 72°30.71'N,

204 157°02.08'W) collected from 111 m, 462 m and 673 water depth, respectively (Fig. 1).

205 The sediments in 01A-GC and in the Holocene part of 05JPC/TC (0–1300 cm) and

206 06JPC (0–935 cm) consist predominantly of homogeneous clayey silt (fine-grained

207 unit). This unit of cores 05JPC and 06JPC is underlain by a more complex

208 lithostratigraphy with laminations and coarse ice rafted debris indicative of

209 glaciomarine environments affected by glacial/deglacial processes ("glaciomarine unit";

210 McKay et al., 2008; Lisé-Pronovost et al., 2009; Polyak et al., 2009).

211 In total 110 samples were collected for mineralogical analysis from core 01A-GC at

212 intervals averaging 5 cm, equivalent to approximately 80–90 years (see chronology

213 description below), down to a depth of 545 cm (ca. 9.3 ka). In core 05JPC/TC, 44

214 samples were collected from fine-grained unit at intervals averaging 30 cm (equivalent

215 to approximately 210–220 years) down to a depth of 1286 cm (ca. 9.3 ka), and 7

216 samples were collected from the underlying glaciomarine sediments. In core 06JPC, 79

217   samples were collected from fine-grained unit at intervals of 10 cm (equivalent to

218   approximately 90 years) down to a depth of 937 cm (ca. 8.0 ka), and 46 samples were

219   collected from the underlying glaciomarine unit.

220   We also analyzed 16 surface sediment samples (0–1 cm) from the eastern Beaufort

221   Sea near the Mackenzie River delta and 3 surface sediment samples from the western

222   Beaufort Sea to fill the gaps in the dataset of Kobayashi et al. (2016) (Fig. 2). These

223   samples were obtained during the RV Araon cruises in 2013 and 2014 (ARA04C and

224   ARA05C, respectively; supplementary table 1).

225

226   3.2. Chronology

227   Age for core 01A-GC was constrained by seven accelerator mass spectrometry

228   (AMS) ^{14}C ages of mollusc shells (Supplementary Table 2; Stein et al., 2017). The core

229   top in ARA 01-GC may not represent the modern age due to some sediment loss in the

230   coring process. This is indicated by the absence of oxidized brown sediment at the core

231   top, as opposed to a multi-corer collected at the same site. Nevertheless, we believe that

232   the top of 01-GC is close to the sediment surface based on the biomarker distribution.

233   IP$_{25}$ and brassicasterols show a downward decreasing trend in their concentrations in the

234   top 10 cm (Stein et al., 2017). We suppose that this indicates their degradation with

235   burial. A similar extent of brassicasterol concentration decrease occurs also in some of

236   the deeper intervals, but is unique for the upper ~200 cm, while the IP25 decrease at the

237   top is unique for the entire record. Therefore, the core top of 01A-GC was assumed to

238   represent sediment surface in the age-depth model. ^{14}C ages were converted to calendar

239   ages using the CALIB7.0 program and marine13 dataset (Reimer et al., 2013). Local

240   reservoir correction (ΔR) for 01A-GC sited in surface waters was assumed 500 years

241 (McNeely et al., 2006; Darby et al., 2012). The age model was constructed by linear

242 interpolation between the ^{14}C datings (3.1–8.6 ka). Ages below the dated range were

243 extrapolated to the bottom of core (9.3 ka).

244   In core 05JPC/TC, age was constrained by six AMS ^{14}C ages of mollusc shells from

245 core 05JPC (Supplementary Table 2; Barletta et al., 2008; Darby et al., 2009). Local

246 reservoir correction (ΔR) was assumed to be 0 years as the core site is washed by

247 Atlantic intermediate water (Darby et al., 2012). Concurrent age constraints for 05JPC

248 were provided by ^{210}Pb determinations in the upper part (05TC) and paleomagnetic

249 analysis (Barletta et al., 2008; McKay et al., 2008). The age model for core 05JPC/TC

250 was constructed by linear interpolation between the ^{14}C datings (2.4–7.7 ka) as well as

251 the assumed modern age of the 05TC top, with the assumption that the offset of JPC to

252 TC is 75 cm (Darby et al., 2009). Ages below the dated range were extrapolated to the

253 bottom of homogenous fine-grained unit at 1300 cm (9.4 ka).

254   In core 06JPC, age was tentatively constrained by ten paleointensity datums based on

255 regional paleomagnetic chronology and a ^{14}C age of benthic foraminifera (8.16 ka at

256 918 cm) (Supplementary Table 2; Lisé-Pronovost et al., 2009), with the assumption that

257 the offset of JPC to TC is 147 cm (Ortiz et al., 2009). The age model for core 06JPC

258 was constructed by linear interpolation between the paleointensity datums (2.0–7.9 ka).

259

260   3.3. XRD mineralogyMineral composition was analyzed on MX-Labo X-ray

261 diffractometer (XRD) equipped with a CuKα tube and monochromator. The tube

262 voltage and current were 40 kV and 20 mA, respectively. Scanning speed was 4°2θ/min

263 and the data sampling step was 0.02°2θ. Each powdered sample was mounted on a glass

264 holder with a random orientation and X-rayed from 2 to 40°2θ. An additional precise

265   scan with a scanning speed of 0.2°2θ/min and sampling step of 0.01°2θ from 24 to

266   27°2θ was conducted to distinguish chlorite from kaolinite by evaluation of the peaks

267   around 25.1°2θ (Elvelhøi and Rønningsland, 1978). In this study, the

268   background-corrected diagnostic peak intensity was used for evaluating the abundance

269   of each mineral. The relative XRD intensities of quartz at 26.6°2θ (d = 3.4 Å), feldspar

270   including both plagioclase and K-feldspar at 27.7°2θ (d = 3.2 Å), illite including mica at

271   8.8°2θ (d = 10.1 Å), chlorite including kaolinite (called "chlorite+kaolinite" hereafter)

272   at 12.4°2θ (d = 7.1 Å), kaolinite at 24.8 °2θ (d = 3.59 Å), chlorite at 25.1°2θ (d = 3.54

273   Å), and dolomite at 30.9° 2θ (d = 2.9 Å) were determined using MacDiff software

274   (Petschick, 2000) based on the peak identification protocols of Biscaye (1965).

275   The mineral ratios used in this study are defined based on XRD peak intensities (PI)

276   as:

277   Q/F = quartz/feldspar = [PI at 26.6°2θ]/[PI at 27.7°2θ]

278   CK/I = (chlorite+kaolinite)/illite = [PI at 12.4°2θ]/[PI at 8.8°2θ]

279   C/I = chlorite/illite = [PI at 25.1°2θ]/[PI at 8.8°2θ]

280   K/I = kaolinite/illite = [PI at 24.8°2θ]/[PI at 8.8°2θ]

281   The standard error of duplicate analyses in all samples averaged 1.1, 0.08 and 0.05

282   for Q/F, CK/I and C/I ratios, respectively.

283   Clay minerals (less than 2-µm diameter) in core 01A-GC were separated by the

284   settling method based on the Stokes' law (Müller, 1967). To produce an oriented powder

285   X-ray diffractometry (XRD) sample, the collected clay suspensions were

286   vacuum-filtered onto 0.45-µm nitrocellulose filters and dried. Ethylene glycol (50 µl)

287   was then soaked onto the oriented clay on the filters. Glycolated sample filters were

288   stored in an oven at 70°C for four hours and then immediately subjected to XRD

289   analyses. Each sample filter was placed directly on a glass slide and X-rayed with a tube

290   voltage of 40 kV and current of 20 mA. Scanning speed was 0.5°2θ/min and the

291   data-sampling step was 0.02°2θ from 2 to 15°2θ. An additional precise scan with a

292   scanning speed of 0.2°2θ/min and sampling step of 0.01°2θ from 24 to 27°2θ was

293   conducted to distinguish chlorite from kaolinite by evaluation of the peaks around

294   25.1°2θ (Elvelhøi and Rønningsland, 1978). The standard errors of duplicate analyses in

295   all samples averaged 0.05 and 0.06 for CK/I and C/I ratios, respectively.

296   The diffraction intensity of chlorite+kaolinite at 7.1 Å was significantly positively

297   correlated with that of chlorite at 3.54 Å (r = 0.89), but not with that of kaolinite at 3.59

298   Å (r = 0.39) in western Arctic surface sediments (Kobayashi et al., 2016), indicating that

299   the diffraction intensity of chlorite+kaolinite is governed by the amount of chlorite rather

300   than that of kaolinite.

301   Spectral analyses of the downcore Q/F and C/I variability were performed using the

302   maximum entropy method provided in the Analyseries software package (Paillard et al.,

303   1996).

304

305   **4. Results**

306   *4.1. Surface sediments of the Beaufort Sea*

307   Because the dataset of Kobayashi et al. (2016) has only one sample in the eastern

308   Beaufort Sea, we added the data of 16 samples from the eastern Beaufort Sea near the

309   Mackenzie delta and 3 samples from the western Beaufort Sea to fill the gaps in their

310   dataset. More clearly than Kobayashi et al. (2016), the new combined dataset shows that

311   the surface sediments in the eastern Beaufort Sea have the higher Q/F and lower CK/I

312   and C/I ratios than those in the Chukchi Sea (Fig. 2A–C; Supplementary table 1).

313   The Q/F ratio showed a westward decreasing trend from the eastern Beaufort Sea to

314   the East Siberian Sea and its offshore area (Fig. 2D). This supports a notion that

315   quartz-rich but feldspar-poor sediments are derived from the North American margin by

316   the BG circulation, whereas feldspar–rich sediments are delivered to the Chukchi Sea

317   from the Siberian margin by currents along the East Siberian slope (Vogt, 1997; Stein,

318   2008; Darby et al., 2011; Kobayashi et al., 2016).

319   The CK/I and C/I ratios showed a northward decreasing trend in the Chukchi Sea and

320   the Chukchi Borderland (Fig. 2E). These results are consistent with earlier studies

321   showing that illite is a common clay mineral in Arctic sediments (Kalinenko, 2001;

322   Darby et al., 2011), whereas, chlorite is more abundant in the Bering Sea and the

323   Chukchi shelf areas influenced by the BSI (Naidu and Mowatt, 1983; Kalinenko, 2001;

324   Nwaodua et al., 2014; Kobayashi et al., 2016).

325   These trends support the conclusion of Kobayashi et al. (2016) mentioning that the

326   Q/F ratio can be used as a provenance index for the BG circulation reflecting a

327   westward decrease in its intensity, and the CK/I and C/I ratios can be used as a

328   provenance index for the BSI reflecting a northward decrease in its intensity. The

329   provenance and transportation of these detrital minerals are discussed in detail in Naidu

330   and Mowatt (1983), Kalinenko (2001), Nwaodua et al. (2014) and Kobayashi et al.

331   (2016).

332

333   *4.2. Cores 01A-GC, 05JPC/TC and 06JPC*

334   Quartz, feldspar, including plagioclase and K-feldspar, illite, chlorite, kaolinite and

335   dolomite were detected in the study samples. Plagioclase comprises a variety of

336   anorthite to albite. Microscopic observations of smear slides for the study samples

revealed that quartz and feldspar are the two major minerals in the composition of detrital grains.

The variation patterns of the Q/F, C/I, CK/I and K/I ratios are different between fine-grained and glaciomarine units in cores 05JPC/TC and 06JPC (Fig. 3; Supplementary tables 3–5). The ratios of fine-grained unit are relatively stable compared with those in glaciomarine units. The higher Q/F ratio in glaciomarine units is consistent with the finding of previous studies that quartz grains are abundant in the western Arctic sediments delivered from the Laurentide ice sheet during glacial and deglacial periods (Bischof et al., 1996; Bischof and Darby, 1997; Phillips and Grantz, 2001; Kobayashi et al., 2016). Some peaks correspond to dolomite-rich layers ("D" in Fig. 3). Variation in the K/I ratio was associated with that in the Q/F ratio (Fig. 3), which is in harmony with an idea that kaolinite was delivered via the Beaufort Gyre circulation (Kobayashi et al., 2016). The C/I and CK/I ratios are lower in glaciomarine unit than in fine-grained unit in 06JPC (Fig. 3C), which is consistent with the closure of Bering Strait in the last glacial (Elias et al., 1992), but this difference is not significant in 05JPC (Fig. 3B). High amplitude fluctuations were observed in the C/I and CK/I ratios in the fine-grained sediments in 01A-GC and 06JPC (Fig. 3A and C). Similar fluctuations partly appeared in 05JPC/TC despite its lower sampling resolution (Fig. 3B).

The Q/F ratio in cores 01A-GC, 05JPC/TC and 06JPC shows a gradual long-term decrease throughout the Holocene (Fig. 4A). In cores 01A-GC and 06JPC studied in more detail, the Q/F ratio also indicates millennial- to century-scale variability (Fig. 4A). Variations of the 5-point running average highlight millennial-scale patterns (Fig. 4A).

360 The variations are generally asynchronous between both cores on this timescale, which

361 strongly depends on their age-depth models.

362 In core 01A-GC, the CK/I and C/I ratios show a general increase after ca. 9.5 ka with

363 the highest values occurring between 6 and 4 ka, and high ratios around 2.5 ka and 1 ka

364 (Fig. 4B). In core 06JPC, the ratios show a general increase after 9.2 ka with higher

365 values occurring between 6 and 3 ka (Fig. 4B). In core 05JPC/TC, slightly higher ratios

366 occur between 6 and 3 ka after a gradual increase from 9.3 ka (Fig. 4B).

367

368 **5. Discussion**

369 *5.1. Holocene trend in the Beaufort Gyre circulation*

370 The zonal gradient of the Q/F ratio in western Arctic sediments shown in Fig. 2

371 suggests that quartz-rich but feldspar-poor sediments are derived from the North

372 American margin by the BG circulation, whereas feldspar–rich sediments are delivered

373 to the Chukchi Sea from the Siberian margin by currents along the East Siberian slope,

374 and the ratio can be used as an index for the BG circulation reflecting changes in its

375 intensity in sediment-core records (Kobayashi et al., 2016). A consistent upward

376 decrease in the Q/F ratio in three different cores under study (Fig. 4A) suggests that the

377 BG weakened during the Holocene. This pattern is consistent with an orbitally-forced

378 decrease in summer insolation at northern high latitudes from the early Holocene to

379 present. High summer insolation likely melted sea ice in the Canada Basin, in particular

380 in the coastal areas (Fig. 5). The evidence of lower ice concentrations at the Canada

381 Basin margins in the early Holocene was shown in the fossil records of bowhead whale

382 bones from the Beaufort Sea coast (Dyke and Savelle, 2001) and driftwood from

383 northern Greenland (Funder et al., 2011). This condition could decrease the stability of

384 the ice cover at the margins of the Canada Basin, which accelerated the rotation of the

385 BG circulation (Fig. 5), by comparison with observations from recent decades (Shimada

386 et al., 2006). A decrease in summer insolation during the Holocene should have

387 increased the stability of sea-ice cover along the coasts, resulting in the weakening of

388 the BG.

389 Recent observations show that the BG circulation is linked to the AO (Proshutinsky

390 and Johnson, 1997; Rigor et al., 2002). In the negative phase of the AO, the Beaufort

391 High strengthens and intensifies the BG. If the gradual weakening of the BG during the

392 Holocene were attributed to atmospheric circulation only, a concurrent shift in the mean

393 state of the AO from the negative to positive phase would be expected. This view,

394 however, contradicts the existing reconstructions of the AO history showing multiple

395 shifts between the positive and negative phases during the Holocene (e.g., Rimbu et al.,

396 2003; Olsen et al., 2012). We, thus, infer that the decreasing Holocene trend of the BG

397 circulation is attributed not to changes in the AO pattern, but rather to the increasing

398 stability of the sea-ice cover in the Canada Basin.

399 Based on a Holocene sediment record off northeastern Chukchi margin, Darby et al.

400 (2012) suggested strong positive AO-like conditions between 3 and 1.2 ka based on

401 abundant ice-rafted iron oxide grains from the West Siberian shelf. In contrast, a mostly

402 negative AO in the late Holocene can be inferred from mineralogical proxy data

403 indicating a general decline of the BSI after 4 ka (Ortiz et al., 2009), which could be

404 attributed to a stronger Aleutian Low (Danielson et al., 2014) that typically corresponds

405 to the negative AO (Overland et al., 1999). Olsen et al. (2012) also concluded that the

406 AO tended to be mostly negative from 4.2 to 2.0 ka based on a redox proxy record from

407 a Greenland lake. In order to comprehend these patterns, we need to consider not only

408   the atmospheric circulation, but also sea-ice conditions. Based on the Q/F record in this

409   study, summer Arctic sea-ice cover shrank in the early to middle Holocene, so that fast

410   ice containing West Siberian grains could less effectively reach the Canada Basin

411   because sea ice would have melted on the way to the BG (Fig. 5). Later in the Holocene

412   the ice cover expanded, and West Siberian fast ice could survive and be incorporated

413   into the BG (Fig. 5). We infer, therefore, that sediment transportation in the BG is

414   principally governed by the distribution of summer sea ice and the resultant stability of

415   the ice cover in the Canada Basin.

416

417   *5.2. Millennial variability in the BG circulation*

418   In addition to the decreasing long-term trend, the Q/F ratio in 01A-GC and 06JPC

419   clearly displays millennial- to century-scale variability (Fig. 4A). Variation in the Q/F

420   ratio of both 01A-GC and 06JPC indicates a significant periodicity of ~2100 and ~1000

421   years with weak periodicities of ~500 and ~360 years, consistent with prominent

422   periodicities in the variation of total solar irradiance (Fig. 6) (Steinhilber et al., 2009). A

423   comparison with the record of total solar irradiance (Steinhilber et al., 2009) shows a

424   general correspondence, where stronger BG circulation (higher Q/F ratio) corresponds

425   to higher solar irradiance (Fig. 7). A ~200-year phase lag between the solar irradiance

426   and the Q/F ratio in 01A-GC and 06JPC may be attributed to the underestimation of

427   local carbon reservoir effect. This pattern suggests that millennial-scale variability in the

428   BG was principally forced by changes in solar irradiance as the most likely forcing.

429   Proxy records consistent with solar forcing were reported from a number of

430   paleoclimatic archives, such as Chinese stalagmites (Hu et al., 2008), Yukon lake

431   sediments (Anderson et al., 2005) and ice cores (Fisher et al., 2008), as well as marine

432   sediments in the northwestern Pacific (Sagawa et al., 2014) and the Chukchi Sea (Stein

433   et al., 2017). Because solar forcing is energetically much smaller than changes in the

434   summer insolation caused by orbital forcing, we suppose that solar activity did not

435   directly affect the stability of ice cover in the Canada Basin. Alternatively, we suggest

436   that the solar activity signal was amplified by positive feedback mechanisms, possibly

437   through changes in the stability of sea-ice cover and/or the atmospheric circulation in

438   the northern high latitudes.

439   In addition to cycles consistent with the solar forcing, Darby et al. (2012) reported a

440   1,550 year cycle in the Siberian grain variation in the Chukchi Sea record. This cycle

441   was, however, not detected in our data indicative of the BG variation (Fig. 6). This

442   difference suggests that the occurrence of Siberian grains in the Chukchi Sea sediments

443   primarily reflects the formation and transportation of fast ice in the eastern Arctic Ocean

444   rather than changes in the BG circulation.

445

446   *5.3. Holocene changes in the Bering Strait Inflow*

447   Northward decreasing trends in the CK/I and C/I ratios in surface sediments in the

448   Chukchi Sea suggests that chlorite-rich sediments are derived from the northern Bering

449   Sea via Bering Strait, and the ratios can be used as an index for the BSI reflecting

450   changes in its intensity in sediment-core records (Kobayashi et al., 2016). Although the

451   variations of the CK/I and C/I ratios are not identical among three study cores (Fig. 4B),

452   there is a common long-term trend showing a gradual increase from 9 to 4.5 ka and a

453   decrease afterwards (Fig. 4B). Large fluctuations are significant in 01A-GC from 6 to 4

454   ka, and this fluctuation is also seen in 6JPC to some extent (Fig. 4B).

455   The higher CK/I and C/I ratios in core 01A-GC in the middle Holocene correspond to

456   higher linear sedimentation rates estimated by interpolation between ^{14}C dating points,

457   but this correspondence is not seen in cores 05JPC/TC and 06JPC (Fig. 4C). We assume

458   that these higher sedimentation rates at 01A-GC indicate intensified BSI, because fine

459   sediment in the study area is mostly transported by currents from the Bering Sea and

460   shallow southern Chukchi shelf (Kalinenko, 2001; Darby et al., 2009; Kobayashi et al.,

461   2016). The difference of chlorite and sedimentation rate records between 01A-GC and

462   05JPC/06JPC may be related to either 1) variable sediment focusing at different water

463   depths, or 2) redistribution of the BSI water between different branches after passing the

464   Bering Strait. 1) A sediment-trap study demonstrated that shelf-break eddies in winter

465   are important to carry fine-grained lithogenic material from the Chukchi Shelf to the

466   slope areas (Watanabe et al., 2014). This redeposition process may have weakened the

467   BSI signal in slope sediments of 05JPC/06JPC compared with outer shelf sediments of

468   01A-GC. 2) Both the Alaskan Coastal Current (ACC) and the central current can

469   transport sediment particles to the 05JPC/TC and 06JPC area (red and yellow arrows,

470   respectively, in Fig. 1; Winsor and Chapman, 2004; Weingartner et al., 2005). In

471   comparison, the western branch is more likely to carry sediment particles to the site of

472   01A-GC (blue arrow in Fig. 1). Redistribution of the BSI water may have caused

473   different response of BSI signals. Although it is not clear which process made the

474   difference of BSI signals between 01A-GC and 05JPC/06JPC cores, it is highly possible

475   that the sedimentation rate and mineral composition of 01A-GC are more sensitive to

476   changes in BSI intensity than those of two other sites.

477   Diffuse spectral reflectance in core HLY0501-06JPC indicated that chlorite +

478   muscovite content is especially high in the middle Holocene between ca. 4 and 6 ka

479 (Supplementary Fig. S1; Ortiz et al., 2009). However, this pattern was not confirmed by

480 our XRD analysis, where XRD intensities of chlorite and muscovite (detected as illite in

481 this study) as well as the C/I and CK/I ratios did not show an identifiable enrichment

482 between 4 and 6 ka (Supplementary Fig. S1). We need more research to understand the

483 discrepancy of the results.

484

485 *5.4. Millennial variability in the BSI*

486 Variation in the C/I ratio of 01A-GC indicates a significant periodicity of 1900, 1000,

487 510, 400 and 320 years (Fig. 6A). The 1900, 1000 and 510 years are consistent with

488 prominent periodicities in the variation of total solar irradiance (Fig. 6C) (Steinhilber et

489 al., 2009). On the other hand, variation in the C/I ratio of 06JPC indicates a periodicity

490 of 2200, 830 and 440 years (Fig. 6B). The periodicity is different from that in 01A-GC

491 (Fig. 6A). This suggests that there are different agents of BSI signals in cores 01A-GC

492 and 06JPC. In core 01A-GC, 1000-year filtered variation in the C/I ratio is nearly

493 antiphase with those of the Q/F ratio and total solar irradiance (Steinhilber et al., 2009)

494 between 0 and 5 ka (Fig. 7). This suggests that millennial-scale variability in the

495 western branch of the BSI was forced by changes in solar irradiance after 5 ka. Recent

496 observations demonstrated that the BSI flows northwestward, especially when easterly

497 winds prevent the ACC (Winsor and Chapman, 2004). Because the easterly winds drive

498 the BG circulation, this mechanism cannot explain the increase of BSI intensity when

499 the BG weakened. Alternatively, it is also possible that the solar forcing could

500 independently regulate the western branch of the BSI via unknown atmospheric-oceanic

501 dynamics.

502

503   *5.5. Ocean circulation, sea ice and biological production*

504   The BSI, an important carrier of heat to the Arctic, affects sea-ice extent in the

505   Chukchi Sea (e.g., Shimada et al., 2006). Sea-ice concentrations in the Chukchi Sea

506   during the Holocene were reconstructed by dinoflagellate cysts (de Vernal et al., 2005;

507   2008; 2013; Farmer et al., 2011) and biomarker IP_{25} (Polyak et al., 2016; Stein et al.,

508   2017).

509   In central northern Chukchi Sea, IP_{25} records showed that sea-ice concentration

510   indicated by PIP_{25} index in core 01A-GC was lower in 9–7.5 ka and 5.5–4 ka (Fig. 8A;

511   Stein et al., 2017), suggesting less sea-ice conditions in the periods. The low sea-ice

512   concentration during 9–7.5 ka is consistent with the results of previous studies based on

513   dinoflagellate cyst and IP_{25} records showing the sea-ice retreat widely in the Arctic

514   Ocean, which was attributed to higher summer insolation during the early Holocene

515   (Dyke and Savelle, 2001; Vare et al., 2009; de Vernal et al., 2013; Stein et al., 2017). On

516   the other hand, the sea-ice retreat during 5.5–4 ka cannot be explained by higher

517   summer insolation. This period corresponds to that of higher C/I and CK/I ratios

518   indicative of the stronger BSI at 01A-GC (Fig. 8A). This suggests that the strengthened

519   BSI during this period contributed to sea-ice retreat in the central Chukchi Sea.

520   In the northeastern Chukchi Sea, dinoflagellate cyst and biomarker IP_{25} records from

521   several cores in the northeastern Chukchi Sea, including 05JPC, demonstrate that

522   sea-ice concentration in this area was overall higher in the early Holocene than in the

523   middle and late Holocene (Fig. 8; de Vernal et al., 2005; 2008; 2013; Farmer et al.,

524   2011; Polyak et al., 2016). This pattern is in contrast to reconstructions from other

525   Arctic regions that show lower sea-ice concentrations in the early Holocene (de Vernal

526   et al., 2013). This discrepancy suggests that the intensified BG circulation exported

527   more ice from the Beaufort Sea to the northeastern Chukchi Sea margin. Furthermore,

528   the heat transport from the North Pacific to the Arctic Ocean by the BSI was likely

529   weaker in the early Holocene than at later times as indicated by the C/I and CK/I ratios

530   of cores 06JPC and 01A-GC (Fig. 8). We infer that this combination of stronger BG

531   circulation and weaker BSI in the early Holocene resulted in increased sea-ice

532   concentration in the northeastern Chukchi Sea despite high insolation levels (Fig. 5). In

533   comparison, intense BSI, a crucial agent of heat transport from the North Pacific to the

534   Arctic Ocean, along with weaker BG in the middle Holocene likely reduced sea-ice

535   cover in the Chukchi Sea. During the late Holocene, characterized by the weakest BG

536   and moderate BSI, sea-ice concentrations were intermediate and strongly variable (Fig.

537   8; de Vernal et al., 2008, 2013; Polyak et al., 2016).

538   The nutrient supply by the BSI potentially affects marine production in the Chukchi

539   Sea. We tested this possibility to compare our BSI record with marine production

540   records from cores 01A-GC (Park et al., 2016; Stein et al., 2017). Isoprenoid GDGTs

541   and brassicasterol showed concentration maxima during the periods between 8 and 7.5

542   ka and 6 and 4.5 ka (Fig. 8A). Isoprenoid GDGTs are produced by marine Archaea

543   (Nishihara et al., 1987) that use ammonia, urea and organic matter in the water column

544   (Qin et al., 2014). Brassicasterol is known as a sterol which is abundant in diatoms

545   (Volkman et al., 1986). Their abundance can, thus, be used as proxies to indicate marine

546   production in the water column. The periods with abundant isoprenoid GDGTs and

547   brassicasterol corresponded to the periods of low PIP_{25} indicative of less sea ice (Fig.

548   8A). This correspondence suggests that the biological productivity increased with the

549   retreat of sea ice in the Chukchi Sea during the middle Holocene. The BSI indices, the

550   C/I and CK/I ratios, showed a maximum between 6 and 4 ka, which corresponded to the

551 periods of high marine production, but the corresponding maximum between 8 and 6.5

552 ka is not significant. Also, correspondence between the BSI indices and biomarker

553 concentrations are not clear after 4 ka. This suggests that marine production was not a

554 simple response to nutrient supply but was affected by other processes such as the

555 increase of irradiance in the water column (Frey et al., 2011; Lee and Whitledge, 2005)

556 and wind-induced mixing that replenishes sea surface nutrients (Carmack et al., 2006).

557

558 *5.6. Causes of BSI variations*

559 Chukchi Sea sedimentary core records indicate a considerable variability in the BSI

560 intensity, with a common long-term trend of a gradual increase from 9 to 4.5 ka and a

561 decrease afterwards (Fig. 4B). Below we discuss the possible controls on this

562 variability.

563 The timing of the initial postglacial flooding of the ~50-m-deep Bering Strait was

564 estimated as between ca. 12 and 11 ka (Elias et al., 1992; Keigwin et al., 2006;

565 Jakobsson et al., 2017). Gradual intensification of the BSI inferred from the increase in

566 chlorite content from ca. 9 to 6 ka may have been largely controlled by the widening

567 and deepening of the Bering Strait with rising sea level, although other factors as

568 discussed below yet need to be tested. After the sea level rose to nearly present position

569 by ca. 6 ka, its influence on changes in the BSI volume was negligible.

570 The possible driving forces of the BSI at full interglacial sea level may include

571 several controls. One is related to the sea surface height difference between the Pacific

572 and Atlantic Oceans regulated by the atmospheric moisture transport from the Atlantic

573 to the Pacific Ocean across Central America (Stigebrandt, 1984). Increase in this

574 moisture transport during warm climatic intervals (Leduc et al., 2007; Richter and Xie,

575 2010; Singh et al., 2016) may have intensified the BSI. Salinity proxy data for the last

576 90 ka from the Equatorial East Pacific confirm increased precipitation during warm

577 events, but also show the trans-Central America moisture transport may operate

578 efficiently only during intervals with a northerly position of the Intertropical

579 Convergence Zone due to orographic constraints (Leduc et al., 2007). The existing

580 Holocene salinity records from the North Pacific (e.g., Sarnthein et al., 2004) do not yet

581 provide sufficient material to test the impact of these changes on the BSI.

582 Interplay of the global wind field and the AMOC has been proposed as another

583 potential control on the BSI (De Boer and Nof, 2004; Ortiz et al., 2012). Results of an

584 analytical ocean modeling experiment (Sandal and Nof, 2008) based on the island rule

585 (Godfrey, 1989) suggest that weaker Subantarctic Westerlies in the middle Holocene

586 could decrease the near surface, cross-equatorial flow from the Southern Ocean to the

587 North Atlantic, thus enhancing the BSI and Arctic outflow into the Atlantic. This

588 hypothesis waits to be tested more thoroughly, including robust proxy records of the

589 Subantarctic Westerlies over the Southern Ocean.

590 Finally, BSI can be controlled by the regional wind patterns in the Bering Sea

591 (Danielson et al., 2014), as explained above in Section 2.1. Oceanographic observations

592 of 2000–2011 clearly show a decadal response of the BSI to a change in the sea level

593 pressure in the Aleutian Basin affecting the dynamic sea surface height along the Bering

594 Strait pressure gradient. In order to conclude if this relationship holds on longer time

595 scales, longer-term records are needed from areas affected by the BSI and the Bering

596 Sea pressure system.

597 A number of proxy records from the Bering Sea and adjacent regions, both marine

598 and terrestrial, have been used to characterize paleoclimatic conditions related to

changes in the Bering Sea pressure system (e.g., Barron et al., 2003; Anderson et al., 2005; Katsuki et al., 2009; Barron and Anderson, 2011; Osterberg et al., 2014). Various proxies used in these records consistently show that the Aleutian Low was overall weaker in the middle Holocene than in the late Holocene, opposite to the BSI strength inferred from our Chukchi Sea data (Fig. 4B). For example, multi-proxy data from the interior Alaska and adjacent territories (Kaufman et al., 2016, and references therein) indicate overall drier and warmer conditions in the middle Holocene, consistent with weaker Aleutian Low and stronger BSI. Diatom records from southern Bering Sea indicate more abundant sea ice in the middle Holocene, also suggestive of a weaker Aleutian Low (Katsuki et al., 2009). Alkenone and diatom records from the California margin show that the sea surface temperature was lower in the middle Holocene, suggesting stronger northerly winds indicative of weaker Aleutian Low (Barron et al., 2003). Intensification of the Aleutian Low in the late Holocene, which follows from these results, would have decreased sea level pressure in the Aleutian Basin, and thus the strength of the BSI, consistent with overall lower BSI after ca. 4 ka inferred from the Chukchi Sea sediment-core data (Fig. 4). Considerable climate variability of the Bering Sea region captured in the upper Holocene records, some of which have very high temporal resolution, is also closely linked to the pressure system changes (Anderson et al., 2005; Porter, 2013; Osterberg et al., 2014; Steinman et al., 2014). In particular, weakening of the Aleutian Low is reflected in Alaskan ice (Porter, 2013; Osterberg et al., 2014) and lake cores (Anderson et al., 2005; Steinman et al., 2014) at intervals centered around ca. 2 and 1–0.5 ka BP, which may correspond to BSI increases in the Chukchi core 01A-GC at ca. 2.5 and 1 ka BP (Fig. 4), considering the uncertainties of the sparse age constraints in the upper Holocene and/or underestimation

623 of reservoir ages. Overall, the Aleutian Low control on the BSI on century to millennial

624 time scales is corroborated by ample proxy data in comparison with the other potential

625 controls, although more evidence is still required for a comprehensive interpretation.

626

627 *6. Summary and Conclusions*

628   Distribution of minerals in surficial bottom sediments from the Chukchi Sea shows

629 two distinct trends: an East-West gradient in quartz/feldspar ratios along the shelf

630 margin, and a northwards decrease in the chlorite contents. These trends are consistent

631 with the propagation of the Beaufort Gyre circulation in the western Arctic Ocean and

632 the Bering Strait inflow to the Chukchi Sea, respectively. Application of these

633 lithological proxies to sedimentary records from the north-central and northeastern parts

634 of the Chukchi Sea allows for an identification of the Holocene paleoceanographic

635 patterns with century to millennial resolution. Results of the identified Holocene

636 changes in the BG circulation and the BSI are summarized in Table 1.

637   The inferred BG weakening during the Holocene, likely driven by the

638 orbitally-controlled summer insolation decrease, indicates basin-wide changes in the

639 Arctic current system and suggests that the stability of sea ice is a key factor regulating

640 the Arctic Ocean circulation on the long-term (e.g., millennial) time scales. This

641 conclusion helps to better understand a dramatic change in the BG circulation during the

642 last decade, probably caused by sea-ice retreat along the margin of the Canada Basin

643 and a more efficient transfer of the wind momentum to the ice and underlying waters

644 (Shimada et al., 2006). These results suggest that the rotation of the BG is likely to be

645 further accelerated by the projected future retreat of summer Arctic sea ice.

646   The identified millennial to multi-centennial variability in the BG circulation

647   (quartz/feldspar ratio) is consistent with Holocene fluctuations in solar irradiance,

648   suggesting that solar activity affected the BG strength on these timescales.

649   Changes in the BSI inferred from the proxy records show a considerable variability

650   between the investigated sediment cores, likely related to interactions of different

651   current branches and depositional processes. Overall, we conclude that after the

652   establishment of the full interglacial sea level in the early Holocene, the BSI variability

653   was largely controlled by the Bering Sea pressure system (strength and position of the

654   Aleutian Low). Details of this mechanism, as well as contributions from other potential

655   BSI controls, such as climatically-driven Atlantic-Pacific moisture transfer and the

656   impact of global wind stress, need to be further investigated. A consistent intensification

657   of the BSI identified in the middle Holocene was associated with a decrease in sea-ice

658   extent and an increase in marine production, indicating a major influence of the BSI on

659   sea ice and biological activity in the Chukchi Sea. In addition, multi-century to

660   millennial fluctuations, presumably controlled by solar activity, are discernible in core

661   01A-GC that has been characterized with the highest age resolution.

662

663   **Acknowledgements**

664   We thank all of the captain, crew and scientists of RV *Araon* for their help during the

665   cruise of sampling. We also thank Yu-Hyeon Park, Anne de Vernal, Seth L. Danielson,

666   Julie Brigham-Grette and Kaustubh Thirumalai for valuable discussion, So-Young Kim,

667   Hyo-Sun Ji, Young-Ju Son, Duk-Ki Han and Hyoung-Jun Kim for assistance in coring

668   and subsampling and Keiko Ohnishi for analytical assistance. Comments by Martin

669   Jakobsson, Tomas M. Cronin, and an anonymous reviewer improved greatly this

670 manuscript. The study was supported by a grant-in-aid for Scientific Research (B) the

671 Japan Society for the Promotion of Science, No. 25287136 (to M.Y.) and Basic

672 Research Project (PE16062) of Korean Polar Research Institute and the NRF of Korea

673 Grant funded by the Korean Government (NRF-2015M1A5A1037243) (to S.I.N.).

674

675 **References**

676 Aagaard, K., Weingartner, T.J., Danielson, S. L., Woodgate, R.A., Johnson, G. C., and

677 Whitledge, T.E.: Some controls on flow and salinity in Bering Strait, Geophysical

678 Research Letters, 33, L19602, 2006.

679 Anderson, L, Abbott, M.B., Finney, B.P., and Burns, S.J.: Regional atmospheric

680 circulation change in the North Pacific during the Holocene inferred from lacustrine

681 carbonate oxygen isotopes, Yukon Territory, Canada, Quaternary Research, 64, 21–

682 35, 2005.

683 Barletta, F. et al.: High resolution paleomagnetic secular variation and relative

684 paleointensity records from the western Canadian Arctic: implication for Holocene

685 stratigraphy and geomagnetic field behaviour, Canadian Journal of Earth Sciences,

686 45, 1265–1281, 2008.

687 Barron, J.A. and Anderson, L.: Enhanced Late Holocene ENSO/PDO expression along

688 the margins of the eastern North Pacific, Quaternary International, 235, 3–12, 2011.

689 Barron, J.A., Heusser, L., Herbert, T., and Lyle, M.: High-resolution climatic evolution

690 of coastal northern California during the past 16,000 years, Paleoceanography, 18,

691 1020, 2003.

692 Biscaye, P.: Mineralogy and sedimentation of recent deep-sea clay in the Atlantic Ocean

693   and adjacent seas and oceans, Geological Society of America Bulletin, 76, 803–832,

694   1965.

695 Bischof, J., Clark, D.L., and Vincent, J.S.: Origin of ice rafted debris: Pleistocene

696   paleoceanography in the western Arctic Ocean, Paleoceanography, 11, 743–756,

697   1996.

698 Bischof, J., and Darby, D.A.: Mid- to Late Pleistocene ice drift in the western Arctic

699   Ocean: Evidence for a different circulation in the Past, Science, 277, 74–78, 1997.

700 Carmack, E., Barber, D., Christensen, J., Macdonald, R., Rudels, B., and Sakshaug, E.:

701   2006. Climate variability and physical forcing of the food webs and the carbon

702   budget on pan-Arctic shelves, Progress in Oceanography, 71, 145–181, 2006.

703 Coachman, L.K., and Aagaard, K.: On the water exchange through Bering Strait,

704   Limnology and Oceanography, 11, 44–59, 1966.

705 Danielson, S.L., Weingartner, T.J., Hedstrom, K.S., Aargaard, K., Woodgate, R.,

706   Curchister, E., and Stabeno, P.J.: Coupled wind-forced controls of the

707   Bering-Chukchi shelf circulation and the Bering Strait throughflow: Ekman

708   transport, continental shelf waves, and variations of the Pacific-Arctic sea surface

709   height gradient, Progress in Oceanography, 125, 40–61, 2014.

710 Darby, D.A., Ortiz, J.D., Polyak, L., Lund, S., Jakobsson, M., and Woodgate, R.A.: The

711   role of currents and sea ice in both slowly deposited central Arctic and rapidly

712   deposited Chukchi-Alaskan margin sediments, Global and Planetary Change, 68,

713   58–72, 2009.

714   Darby, D.A., Myers, W.B., Jakobsson, M., and Rigor, I.: Modern dirty sea ice

715   characteristic and sources: The role of anchor ice, Journal of Geophysical Research,

716   116, C09008, 2011.

717   Darby, D.A., Ortiz, J.D., Grosch, C.E., and Lund, S.P.: 1,500-year cycle in the Arctic

718   Oscillation identified in Holocene Arctic sea-ice drift, Nature Geoscience, 5, 897–

719   900, 2012.

720   De Boer, A.M. and Nof, D.: The exhaust valve of the North Atlantic, Journal of Climate,

721   17, 417–422, 2004.

722   de Vernal, A., Hillaire-Marcel, C., and Darby, D.A.: Variability of sea ice cover in the

723   Chukchi Sea (western Arctic Ocean) during the Holocene, Paleoceanography, 20,

724   PA4018, doi:10.1029/2005PA001157, 2005.

725   de Vernal A, Hillaire-Marcel C, Solignac S, et al.: Reconstructing sea ice conditions in

726   the Arctic and sub-Arctic prior to human observations, Geophysical Monograph

727   180, American Geophysical Union, Washington, p. 27–45, 2008.

728   de Vernal, A. et al.: Dinocyst-based reconstructions of sea ice cover concentration

729   during the Holocene in the Arctic Ocean, the northern North Atlantic Ocean and its

730   adjacent seas, Quaternary Science Reviews, 79, 111–121, 2013.

731   Dyke, A.S. and Savelle, J.M.: Holocene history of the Bering Sea bowhead whale

732   (*Balaena mysticetus*) in Its Beaufort Sea summer grounds off southwestern Victoria

733   Island, western Canadian Arctic, Quaternary Research, 55, 371–379, 2001.

734   Elias, S., Short, S.K., and Phillips, R.L.: Paleoecology of late-glacial peats from the

735   Bering land bridge, Chukchi Sea shelf region, northwestern Alaska, Quaternary

736   Research, 38, 371–378, 1992.

737 Elvelhøi, A. and Rønningsland, T.M.: Semiquantitative calculation of the relative

738   amounts of kaolinite and chlorite by X-ray diffraction, Marine Geology, 27,

739   M19-M23, 1978.

740 Farmer, J.R., Cronin, T.M., de Vernal, A., Dwyer, G.S., Keigwin, L.D., and Thunell,

741   R.C.: Western Arctic Ocean temperature variability during the last 8000 years,

742   Geophysical Research Letters, 38, L24602, 2011.

743 Fisher, D., Osterberg, E., Dyke, A., Dahl-Jensen, D., Demuth, M., Zdanowicz, C.,

744   Bourgeois, J., Koerner, R.M., Mayewski, P., Wake, C., Kreutz, K., Steig, E., Zheng,

745   J., Yalcin, K., Goto-Azuma, K., Luckman, B., Rupper, S.: The Mt Logan Holocene–

746   late Wisconsinan isotope record: tropical Pacific–Yukon connections. Holocene, 18,

747   667–677, 2008.

748 Frey, K.E., Perovich, D.K., and Light, B.: The spatial distribution of solar radiation

749   under a melting Arctic sea ice cover, Geophysical Research Letters, 38, L22501,

750   2011.

751 Funder, S. et al.: A 10,000-year record of Arctic Ocean sea-ice variability–View from

752   the beach, Science, 333, 747–750, 2011.

753 Giles, K.A. et al.: Western Arctic Ocean freshwater storage increased by wind-driven

754   spin-up of the Beaufort Gyre, Nature Geoscience, 5, 194–197, 2012.

755 Godfrey, J.S.: A sverdrup model of the depth-integrated flow for the ocean allowing for

756   island circulations, Geophysical and Astrophysical Fluid Dynamics, 45, 89–112,

757   1989.

758 Griffin, G.M. and Goldberg, E.D.: Clay mineral distributions in the Pacific Ocean. In

759   Hill, M.N. (ed) The sea, III, p. 728-741, New York, Interscience Pub., 1963.

760 Gudkovitch, Z.M.: On the nature of the Pacific current in Bering Strait and the cause of

761   its seasonal variations, Deep-Sea Research, 9, 507–510, 1962.

762 Harada, N.: Review: Potential catastrophic reduction of sea ice in the western Arctic

763   Ocean: its impact on biogeochemical cycles and marine ecosystems, Global and

764   Planetary Change, 136, 1–17, 2016.

765 Hu, C., Henderson, G.M., Huang, J., Xie, S., Sun,Y., Johnson, K.R.: Quantification of

766   Holocene Asian monsoon rainfall from spatially separated cave records. Earth and

767   Planetary Science Letters, 266, 221–232, 2008.

768 Jakobsson, M., Pearce, C., Cronin, T.M., Backman, J., Anderson, L.G., Barrientos, N.,

769   Björk, G., Coxall, H., de Boer, A., Mayer, L.A., Mörth, C.-M., Nilsson, J., Rattray,

770   J.E., Stranne, C., Semilietov, I., and O'Regan, M.: Post-glacial flooding of the

771   Beringia land bridge dated to 11,000 cal yrs BP based on new geophysical and

772   sediment records. Climate of the Past Discussions, doi:10.5194/cp-2017-11, 2017.

773 Kaufman, D.S. et al.: Holocene climate changes in eastern Beringia (NW North

774   America) – a systematic review of multi-proxy evidence, Quaternary Science

775   Reviews, 147, 312–339, 2016.

776 Kalinenko, V.V.: Clay minerals in sediments of the Arctic Seas. Lith. Min. Res. 36, 362–

777   372. Translated from Litologiya I Poleznye Iskopaemye 4, 418–429, 2001.

778 Katsuki, K., Khim, B.-K., Itaki, T., Harada, N., Sakai, H., Ikeda, T., Takahashi, K.,

779   Okazaki, Y., and Asahi, H.: Land–sea linkage of Holocene paleoclimate on the

780   Southern Bering Continental Shelf, The Holocene, 19, 747–756, 2009.

781 Keigwin, L.D., Donelly, J.P., Cook, M.S., Driscoll, N.W., and Brigham-Grette, J.: Rapid

782   sea-level rise and Holocene climate in the Chukchi Sea, Geology, 34, 861–864,

783   2006.

784 Kobayashi, D., Yamamoto, M., Irino, T., Nam, S.-I., Park, Y.-H., Harada, N., Nagashima,

785   K., Chikita, K., and Saitoh, S.-I.: Distribution of detrital minerals and sediment

786   color in western Arctic Ocean and northern Bering Sea sediments: Changes in the

787   provenance of western Arctic Ocean sediments since the last glacial period, Polar

788   Science, 10, 519–531, 2016.

789 Leduc, G., Vidal, L., Tachikawa, K., Rostek, F., Sonzogni, C., Beaufort, L. and Bard, E.:

790   Moisture transport across Central America as a positive feedback on abrupt climatic

791   changes, Nature, 445, 908–911, doi:10.1038/nature05578, 2007.

792 Lee, S.H., and Whitledge, T.E.: Primary and new production in the deep Canada Basin

793   during summer 2002, Polar Biology, 28, 190–197, 2005.

794 Lisé-Pronovost, A., St-Onge, G., Brachfeld, S., Barletta, F., and Darby, D.:

795   Paleomagnetic constraints on the Holocene stratigraphy of the Arctic Alaskan margin,

796   Global and Planetary Change, 68, 85–99, 2009.

797 McKay, J. L. et al.: Holocene fluctuations in Arctic sea-ice cover: dinocyst-based

798   reconstructions for the eastern Chukchi Sea, Canadian Journal of Earth Sciences, 45,

799   1377–1397, 2008.

800 McNeely, R., Dyke, A.S., and Southon, J.R.: Canadian marine reservoir ages,

801   preliminary data assessment, Open File Report-Geological Survey of Canada, 5049,

802   no. 3, 2006.

803 Miller, G.H., Alley, R.B., Brigham-Grette, J., Fitzpatrick, J.J., Polyak, L., Serreze, M.C.,

804   White, J.W.C.: Arctic amplification: can the past constrain the future? Quaternary

805   Science Reviews, 29, 1779–1790, 2010.

806 Müller, G.: Methods in Sedimentary Petrology, Scweizerbart Science Publishers, 283p,

807   Stuttgart, 1967.

808   Naidu, A.S., Creager, J.S., and Mowatt, T.C.: Clay mineral dispersal patterns in the

809   North Bering and Chukchi Seas, Marine Geology, 47, 1-15, 1982.

810   Naidu, A.S. and Mowatt, T.C.: Sources and dispersal patterns of clay minerals in surface

811   sediments from the continental shelf areas off Alaska, Geological Society of

812   America Bulletin, 94, 841–854, 1983.

813   Nishino, S., Shimada, K., Itoh, M., and Chiba, S.: Vertical double silicate maxima in the

814   sea-ice reduction region of the western Arctic Ocean: implications for an enhanced

815   biological pump due to sea-ice reduction, Journal of Oceanography, 60, 871–883,

816   2009.

817   Nishihara, M., Morri, H., and Koga, Y.: Structure determination of a quartet of novel

818   tetraether lipids from Methanobacterium thermoautotrophicum, Journal of

819   Biochemistry, 101, 1007–1015, 1987.

820   Nwaodua, E., Ortiz, J.D., and Griffith, E.M.: Diffuse spectral reflectance of surficial

821   sediments indicates sedimentary environments on the shelves of the Bering Sea and

822   western Arctic, Marine Geology, 355, 218–233, 2014.

823   Olsen, J., Anderson, N.J., and Knudsen, M.F.: Variability of the North Atlantic

824   Oscillation over the past 5,200 years, Nature Geoscience, 5, 808–812, 2012.

825   Ortiz, J.D., Polyak, L., Grebmeier, J.M., Darby, D., Eberl, D.D., Naidu, S., and Nof, D.:

826   Provenance of Holocene sediment on the Chukchi-Alaskan margin based on

827   combined diffuse spectral reflectance and quantitative X-Ray Diffraction analysis,

828   Global Planetary Change, 68, 73–84, 2009.

829   Ortiz, J.D., Nof, D., Polyak, L., St-Onge, G., Lisé-Pronovost, A., Naidu, S., Darby, D.,

830   and Brachfeld, S.: The late Quaternary flow through the Bering Strait has been

831   forced by the Southern Ocean winds, Journal of Physical Oceanography, 42, 2014–

832   2029, 2012.

833   Osterberg, E.C., Mayewski, P.A., Fisher, D.A., Kreutz, K.J., Maasch, K.A., Sneed, S.B.,

834   and Kelsey, E.: Mount Logan ice core record of tropical and solar influences on

835   Aleutian Low variability: 500–1998 A.D. Journal of Geophysical Research,

836   Atmosphere, 119, 11,189–11,204, doi:10.1002/2014JD021847, 2014.

837   Overland, J.O., Adams, J. M., and Bond, N.: Decadal variability of the Aleutian Low

838   and its relation to high-latitude circulation, Journal of Climate, 12, 1542–1548,

839   1999.

840   Paillard, D., Labeyrie, L., and Yion, P.: Macintosh program performs time-series

841   analysis, EOS Trans. AGU 77, 379, 1996.

842   Park, Y.-H., Yamamoto, M., Polyak, L., and Nam, S.-I.: Glycerol dialkyl glycerol

843   tetraether variations in the northern Chukchi Sea, Arctic Ocean, during the

844   Holocene, Biogeosciences Discussion, doi:10.5194/bg-2016-529, 2016.

845   Petschick, R.: MacDiff 4.2.6. [online] available at

846   http://www.geol-pal.uni-frankfurt.de/Staff/Homepages/Petschick/MacDiff/MacDiff

847   %20Latest%20infoE.html, 2000.

848   Phillips, R.P., and Grantz, A.: Regional variations in provenance and abundance of

849   ice-rafted clasts in Arctic Ocean sediments: implications for the configuration of

850   late Quaternary oceanic and atmospheric circulation in the Arctic, Marine Geology

851   172, 91–115, 2001.

852   Pickart, R.S.: Shelfbreak circulation in the Alaskan Beaufort Sea: Mean structure and

853   variability, Journal of Geophysical Research 109, C04024, 2004.

854 Pickart, R.S., Pratt, L.J., Torres, D.J., Whitledge, T.E., Proshutinsky, A.Y., Aagaard, K.,

855   Agnewd, T.A., Moore, G.W.K., and Dail, H.J.: Evolution and dynamics of the flow

856   through Herald Canyon in the western Chukchi Sea, Deep-Sea Research II, 57, 5–

857   26, 2010.

858 Polyak, L., Bischof, J., Ortiz, J.D., Darby, D.A., Channell, J.E.T., Xuan, C., Kaufman,

859   D.S., Løvile, R., Schneider, D., Eberl, D.D., Adler, R.E., and Council, E.A.: Late

860   Quaternary stratigraphy and sedimentation patterns in the western Arctic Ocean,

861   Global and Planetary Change, 68, 5–17, 2009.

862 Polyak, L., Belt, S., Cabedo-Sanz, P., Yamamoto, M., and Park, Y.-H.: Holocene

863   sea-ice conditions and circulation at the Chukchi-Alaskan margin, Arctic Ocean,

864   inferred from biomarker proxies, The Holocene, 26, 1810–1821, 2016.

865 Porter, S.E.: Assessing whether climate variability in the Pacific Basin influences the

866   climate over the North Atlantic and Greenland and modulates sea ice extent, Ph.D.

867   Thesis, Ohio State University, 222 p, 2013.

868 Proshutinsky, A.Y. and Johnson, M.A.: Two circulation regimes of the wind-driven

869   Arctic Ocean, Journal of Geophysical Research, 102 (C6), 12493–12514, 1997.

870 Qin, W., Amin, S.A., Martens-Habbena, W., Walker, C.B., Urakawa, H., Devol, A.H.,

871   Ingalls, A.E., Moffett, J.M., Armbrust, E.V., and Stahl, D.A.: Marine

872   ammonia-oxidizing achaeal isolates display obligate mixotrophy and wide ecotypic

873   variation. Proceedings of the National Academy of Science, 111, 12504–12509,

874   2014.

875 Reimer, P.J., et al.: Intcal13 and Marine13 radiocarbon age calibration curves 0–50,000

876   years cal BP., Radiocarbon, 55, 1869–1887, 2013.

877   Richter, I. and Xie, S.: Moisture transport from the Atlantic to the Pacific basin and its

878   response to North Atlantic cooling and global warming, Climate Dynamics, 35,

879   551–566, doi:10.1007/s00382-009-0708-3, 2010.

880   Rigor, I. G. et al.: Response of sea ice to the Arctic Oscillation, Journal of Climate, 15,

881   2648–2663, 2002.

882   Rimbu, N., Lohmann, G., Kim, J.-H., Arz, H.W., and Schneider, R.: Arctic/North

883   Atlantic Oscillation signature in Holocene sea surface temperature trends as

884   obtained from alkenone data, Geophysical Research Letters, 30, 1280.

885   doi:10.1029/2002GL016570, 2003.

886   Roach, A.T., Aagaard, K., Pease, C.H., Salo, S.A., Weingartner, T., Pavlov, V., and

887   Kulakov, M.: Direct measurements of transport and water properties through

888   Bering Strait, Journal of Geophysical Research, 100, 18433–18457, 1995.

889   Sagawa, T., Kuwae, M., Tsuruoka, K., Nakamura, Y., Ikehara, M., and Murayama, M.:

890   Solar forcing of centennial-scale East Asian winter monsoon variability in the

891   mid-to late Holocene. Earth and Planetary Science Letters, 395, 124–135, 2014.

892   Sakshaug, E.: Primary and secondary production in the Arctic ocean, In: Stein, R.,

893   Macdonald, R.W. (Eds.), The Organic Carbon Cycle in the Arctic Ocean, Springer,

894   Berlin, pp. 57–81, 2004.

895   Sandal, C. and Nof, D.: The Collapse of the Bering Strait Ice Dam and the Abrupt

896   Temperature Rise in the Beginning of the Holocene, Journal of Physical

897   Oceanography, 38, 1979–1991, 2008.

898   Sarnthein, M., Gebhardt, H., Kiefer, T., Kucera, M. Cook, M., and Erlenkeuserd, H.:

899   Mid Holocene origin of the sea-surface salinity low in the subarctic North Pacific,

900   Quaternary Science Reviews, 23, 2089–2099, 2004.

901   Screen, J.A. and Simmonds, I.: The central role of diminishing sea ice in recent Arctic

902   temperature amplification, Nature, 464, 1334–1337, 2010.

903   Shimada, K., Carmack, E., Hatakeyama, K., and Takizawa, T.: Varieties of shallow

904   temperature maximum waters in the Western Canadian Basin of the Arctic Ocean,

905   Geophysical Research Letters, 28, 3441–3444, 2001.

906   Shimada, K., Kamoshida, T., Itoh, M., Nishino, S., Carmack, E., McLaughlin, F.,

907   Zimmermann, S., and Proshutinsky, A.: Pacific Ocean inflow: Influence on

908   catastrophic reduction of sea ice cover in the Arctic Ocean, Geophysical Research

909   Letters, 33, L08605, 2006.

910   Shtokman, V.B.: Vliyanie vetra na techeniya v Beringovo Prolive, prichiny ikh

911   bol'shikh skorostei i preobladayueshego severnogo napravleniya, Trans. Inst.

912   Okeanolog., Akad. Nauk SSSR, 25, 171– 197, 1957.

913   Singh, H.K.A., Donohoe, A., Bitz, C.M., Nusbaumer, J., and Noone, D.C.: Greater

914   aerial moisture transport distances with warming amplify interbasin salinity

915   contrasts.   Geophysical   Research   Letters   43,   8677–8684,

916   doi:10.1002/2016GL069796, 2016.

917   Stein R.: Developments in Marine Geology: Arctic Ocean Sediments: Processes,

918   Proxies, and Paleoenvironment, Elsevier, Amsterdam, 529p, 2008.

919   Stein, R., Fahl, K., Schade, I., Nanerung, A., Wassmuth, S., Niessen, F., and Nam, S.-I.:

920   Holocene variability in sea ice cover, primary production, and Pacific-Water inflow

921   and climate change in the Chukchi and East Siberian Seas (Arctic Ocean), Journal

922   of Quaternary Science, 32, 362–379, 2017.

923   Steinman, B.A., Abbott, M.B., Mann, M.E., Ortiz, J.D., Feng, S., Pompeani, D.P.,

924   Stansell, N.D., Anderson, L., Finney, B.P., and Bird, B.W.: Ocean-atmosphere

925   forcing of centennial hydroclimate variability in the Pacific Northwest,

926   Geophysical Research Letters, 41, doi:10.1002/2014GL059499, 2014.

927   Steinhilber, F., Beer, J., and Fröhlich, C.: Total solar irradiance during the Holocene,

928   Geophysical Research Letters, 36, L19704, doi:10.1029/2009GL040142, 2009.

929   Stigebrandt, A.: The North Pacific: A global-scale estuary, Journal of Physical

930   Oceanography, 14, 464–470, 1984.

931   Vare L.L., Masse G., and Gregory, T.R.: Sea ice variations in the central Canadian

932   Arctic Archipelago during the Holocene, Quaternary Science Reviews, 28, 1354–

933   1366, 2009.

934   Viscosi-Shirley, C., Mammone, K., Pisias, N., and Dymond, J.: Clay mineralogy and

935   multi-element chemistry of surface sediments on Siberian-Arctic shelf: implications

936   for sediment provenance and grain size sorting, Continental Shelf Research, 23,

937   1175–1200, 2003.

938   Vogt, C.: Regional and temporal variations of mineral assemblages in Arctic Ocean

939   sediments as climatic indicator during glacial/interglacial changes, Reports on Polar

940   Research, 251, 1–309, 1997.

941   Volkman, J.K.: A review of sterol markers for marine and terrigenous organic matter,

942   Organic Geochemistry, 9, 83–99, 1986.

943   Wahsner, M., Müller, C., Stein, R., Ivanov, G., Levitan, M., Shekekhova, E., and

944   Tarasov, G.: Clay-mineral distribution in surface sediments of Eurasian Arctic

945   Ocean and continental margin as indicator for source areas and transport pathways

946   – a synthesis, Boreas, 28, 216–233, 1999.

947 Walsh, J.J., and Dieterle, D.A.: CO_2 cycling in the coastal ocean. I. A numerical analysis

948   of the southeastern Bering Sea, with applications to the Chukchi sea and the

949   northern Gulf of Mexico, Progress in Oceanography, 34, 335–392, 1994.

950 Watanabe, E., Onodera, J., Harada, N., Honda, M., Kimoto, K., Kikuchi, T., Nishino, S.,

951   Matsuno, K., Yamaguchi, A., Ishida, A., and Kishi, J.M.: Enhanced role of eddies

952   in the Arctic marine biological pump. Nature Communications,

953   http://dx.doi.org/10.1038/ncomms4950, 2014.

954 Weingartner, T., Aagaard, K., Woodgate, R., Danielson, S., Sasaki, Y., and Cavalieri, D.:

955   Circulation on the north central Chukchi Sea shelf, Deep-Sea Research II, 52,

956   3150–3174, 2005.

957 Winsor, P. and Chapman, D.C.: Pathways of Pacific water across the Chukchi Sea: A

958   numerical model study, Journal of Geophysical Research, 109, C03002,

959   doi:10.1029/2003JC001962, 2004.

960 Woodgate, R.A., Weingartner, T.J., and Lindsay, R.: Observed increases in Bering Strait

961   fluxes from the Pacific to the Arctic from 2001 to 2011 and their impacts on the

962   Arctic Ocean water column, Geophysical Research Letters, 39, L24603, 2012.

963 Yamamoto-Kawai, M., Carmack, E., and McLaughlin, F.: Nitrogen balance and Arctic

964   throughflow, Nature, 443, 43, 2006

965

Table 1. Summary of Holocene variability in the BG and BSI in northern Chukchi Sea

Current system	Holocene trends	Multi-centennial to Millennial cyclicity
Beaufort Gyre (BG) circulation	Gradual weakening in response to decreasing summer insolation	0.36, 0.5, 1, and 2-ky cycles paced by changes in solar activity
Bering Strait inflow (BSI)	Geographically variable. Mid-Holocene strengthening evident at the 01A-GC site, presumably due to weaker Aleutian Low	Geographically variable. ~0.36, 0.5, 1, and 2-kyr cycles paced by changes in solar activity are identifiable in 01A-GC

966

 Figure captions

968

969   Fig. 1. Index map showing location of cores ARA02B 01A-GC (this study),

970   HLY0501-05JPC/TC (this study and Farmer et al., 2011), HLY0501-06JPC (this study

971   and Ortiz et al., 2009), and HLY0205-GGC19 (Farmer et al., 2011), as well as surface

972   sediment samples (Kobayashi et al., 2016, with additions). BSI = Bering Strait inflow,

973   BC = Barrow Canyon, HN = Hanna Shoal, and HR = Herald Shoal. BG = Beaufort

974   Gyre, ACC = Alaskan Coastal Current, SBC = Subsurface Boundary Current, ESCC =

975   East Siberian Coastal Current, TPD = Transpolar Drift. Red, yellow and blue arrows

976   indicate BSI branches. AO+ and AO– indicate circulation in the positive and negative

977   phases of the Arctic Oscillation, respectively.

978

979   Fig. 2. Spatial distributions of the diffraction intensity ratios of (A) feldspar to quartz

980   (Q/F), and of (B) chlorite+kaolinite and (C) chlorite to illite (CK/I and C/I, respectively)

981   of bulk sediments, and (D) the longitudinal distribution of the Q/F ratio in the western

982   Arctic (>65°N) and (E) the latitudinal distribution of the CK/I and C/I ratios in the

983   Bering Sea and the western Arctic (>150°W). The C/I ratio could not be determined in

984   some coarse-grained sediment samples. Data from Kobayashi et al. (2016) with

985   additions for the Beaufort Sea (See supplementary Table 1 in more detail). The

986   regression lines in panel E show the geographic trends in mineral proxy distribution for

987   the Chukchi Sea. The Bering Sea sediments do not show a systematic pattern, probably

988   reflecting multiple sources of chlorite, such as the Yukon River, Aleutian Island, etc.

989   The enlarged maps of the Mackenzie River delta and Yukon River estuary are shown in

990   supplementary Figs. 1 and 2.

991

Fig. 3. Depth profile in (A) quartz/feldspar (Q/F) ratio, (chlorite + kaolinite)/illite (CK/I), chlorite/illite (C/I) and kaolinite/illite (K/I) ratios with 1σ-intervals (analytical error) and the diffraction intensity of dolomite (D) in cores (A) ARA02B 01A-GC, (B) HLY0501-05JPC/TC and (C) HLY0501-06JPC (Supplementary Tables 2–4). Crosses indicate radiocarbon dates in 01-GC and 5JPC and paleointensity datums in 06JPC. Open circles in Panel B indicate 05TC samples. Note that the depth scale for 01A-GC is doubled for presentation purposes.

999

Fig. 4. Holocene changes in (A) quartz/feldspar (Q/F) ratio and the June insolation at 75°N, (B) (chlorite + kaolinite)/illite (CK/I) and chlorite/illite (C/I) ratios, and (C) linear sedimentation rates (LSR) between age tie points in cores ARA02B 01A-GC, HLY0501-05JPC/TC and HLY0501-06JPC. Note that the age model for 06JPC is very tentative, so that a peak in LSR at ca. 2 ka could be an artifact of spurious age controls.

1005

Fig. 5. Conceputual map showing the distribution of summer sea ice and the rotation of the Beaufort Gyre (BG) in the early, middle and late Holocene, inferred from the quartz/feldspar (Q/F) proxy record. Also shown is the Bering Strait inflow (BSI) intensity inferred from the (chlorite + kaolinite)/illite (CK/I) and chlorite/illite (C/I) ratios. Red arrow indicates the drift path of Kara Sea grains (KSG; Darby et al., 2012).

1011

Fig. 6. Max Entropy power spectra of variation in the quartz/feldspar (Q/F) and chlorite/illite (C/I) ratios in core ARA02B 01A-GC (N=85, m=21) and

1014   HYL0501-06JPC (N=79, m=22) during 1.4–7.9 ka and the total solar irradiance (N=932,

1015   m=140))(Steinhilber et al., 2009) during the last 9.3 ka.

1016

1017   Fig. 7. Detrended variations in the solar irradiance (TSI; Steinhilber et al., 2009), the

1018   quartz/feldspar (Q/F) ratio in logarithmic scale in cores ARA02B 01A-GC and

1019   HYL0501-06JPC and the chlorite/illite (C/I) ratio in core ARA02B 01A-GC during the

1020   Holocene, with 400-year moving averages and 1,000-year filtered variations indicated

1021   by dark colored and black lines, respectively. The detrended values were obtained by

1022   cubic polynomial regression.

1023

1024   Fig. 8. Changes in (A) (chlorite + kaolinite)/illite (CK/I) and chlorite/illite (C/I) ratios,

1025 PIP_{25} (P_DIP_{25} and P_BIP_{25} based on IP_{25} and dinosterol or brassicasterol concentrations)

1026   indices (Stein et al., 2017), and isoprenoid GDGT (Park et al., 2016) and brassicasterol

1027   concentrations (Stein et al., 2017) in core ARA02B 01A-GC, (B) CK/I and C/I ratios in

1028   core HLY0510-5JPC/TC, IP_{25} concentrations in core HLY0510-5JPC (Polyak et al.,

1029   2016), mean annual sea ice cover concentration (scale from 0 to 10) estimated from

1030   dinoflagellate cyst assemblages in cores 05JPC and GGC19 (de Vernal et al., 2013).

1031
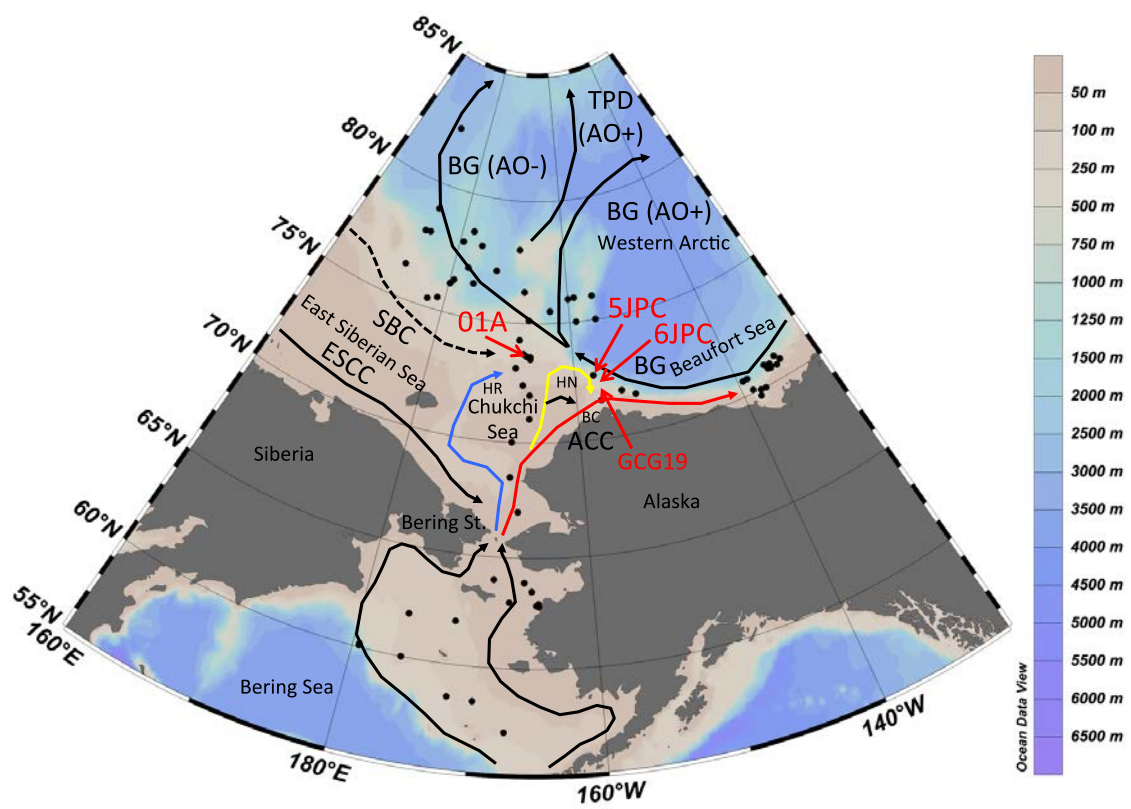
1032

1033

1034   Fig. 1

1035
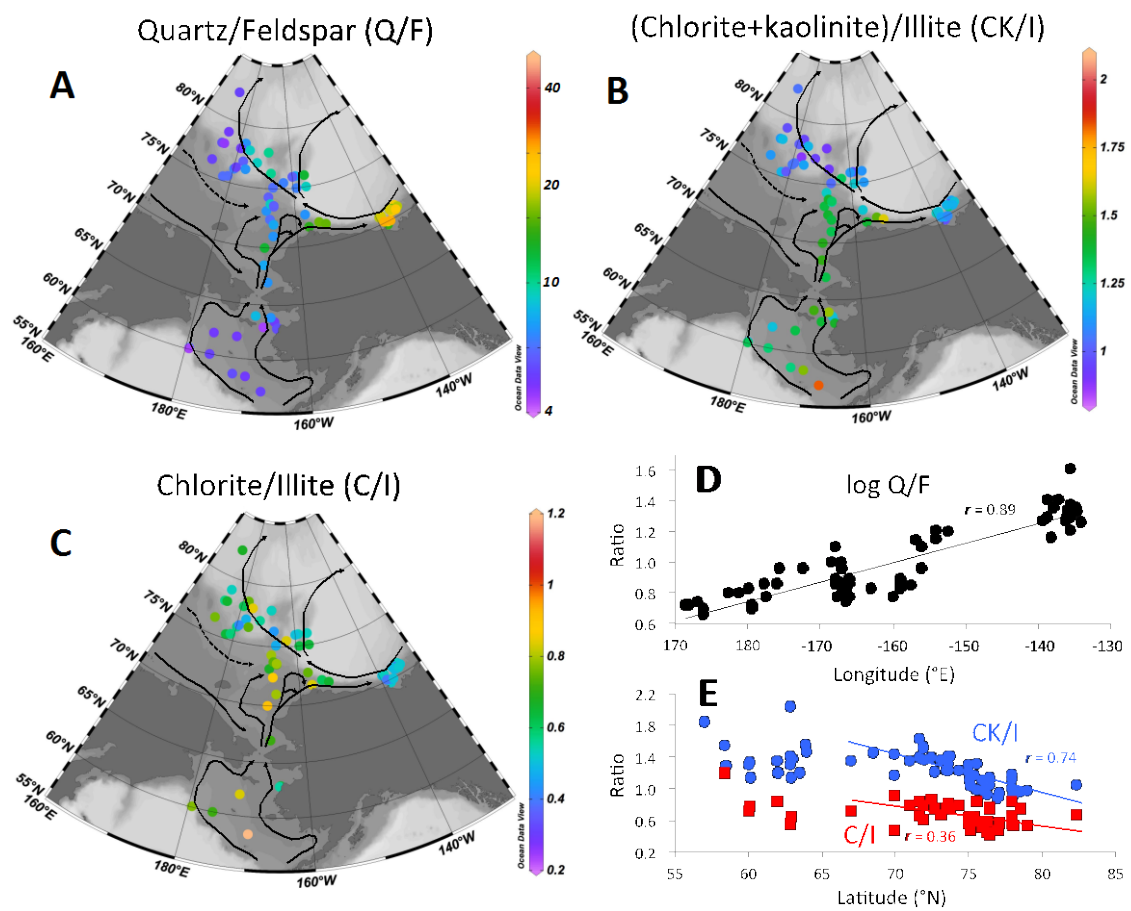
1036

1037   Fig. 2

1038
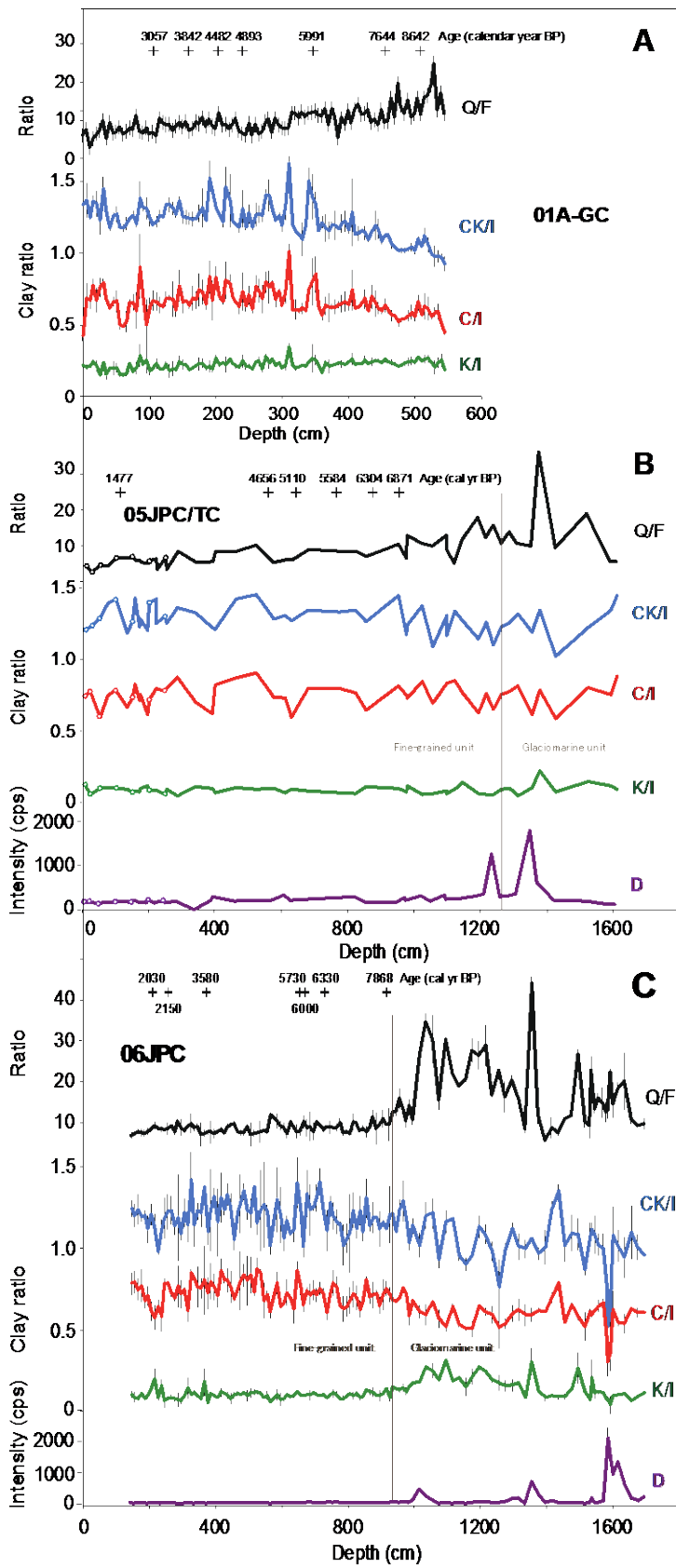
1039
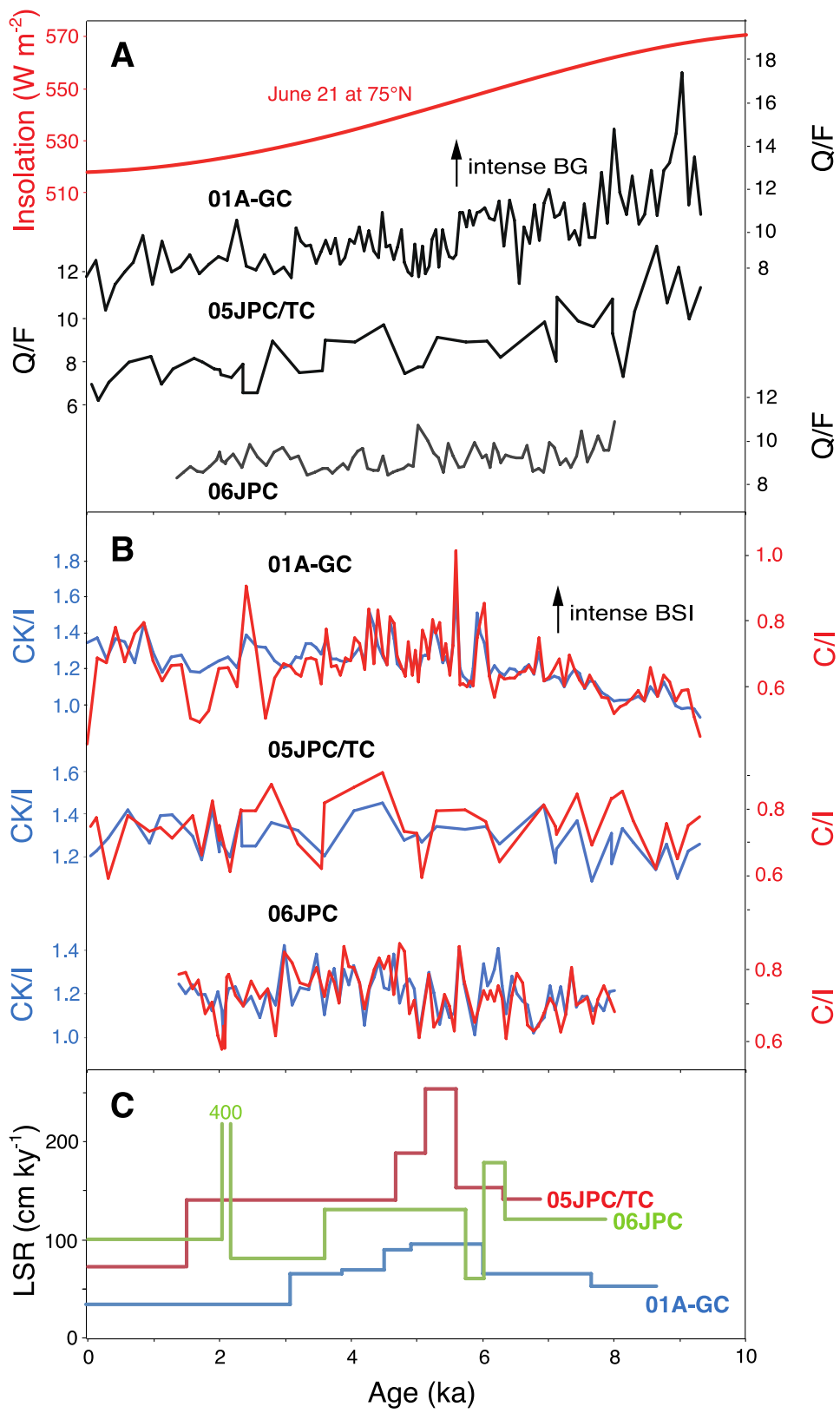
1040 Fig. 3
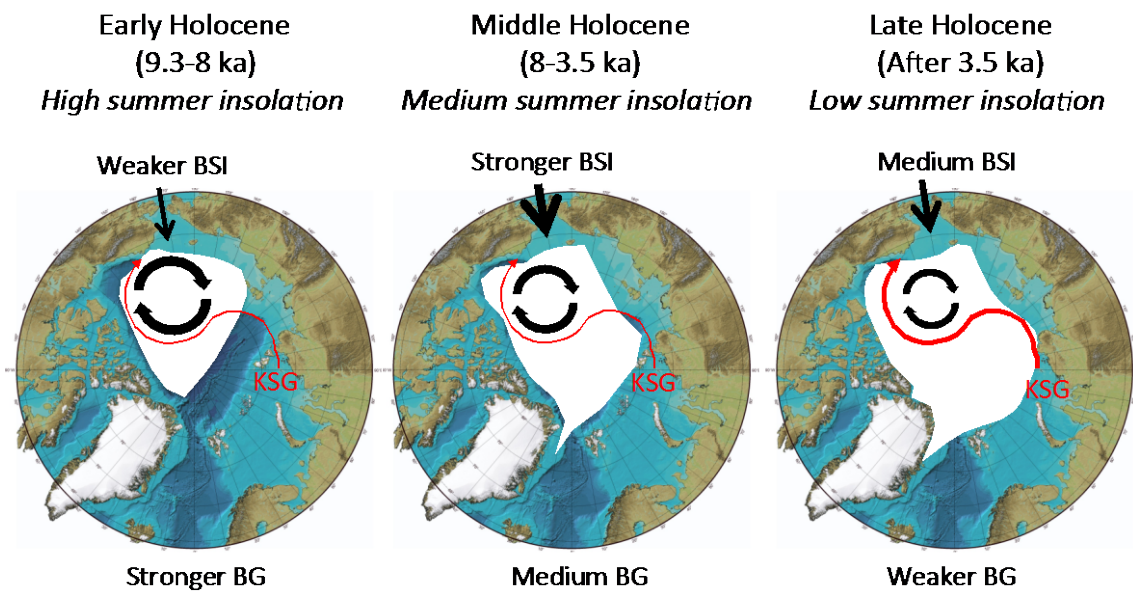
1044   Fig. 5

1045
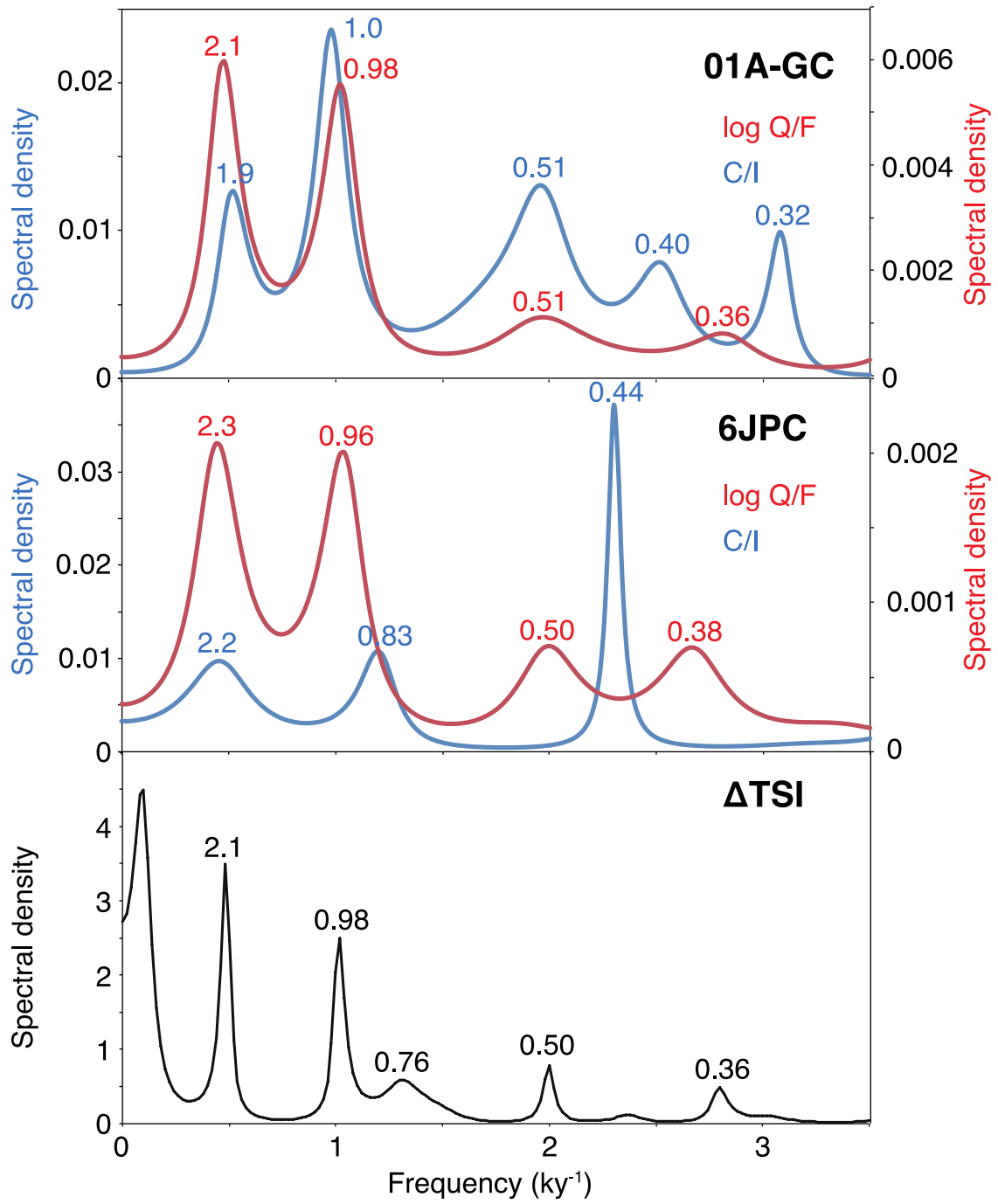
1046

1047   Fig. 6

1048
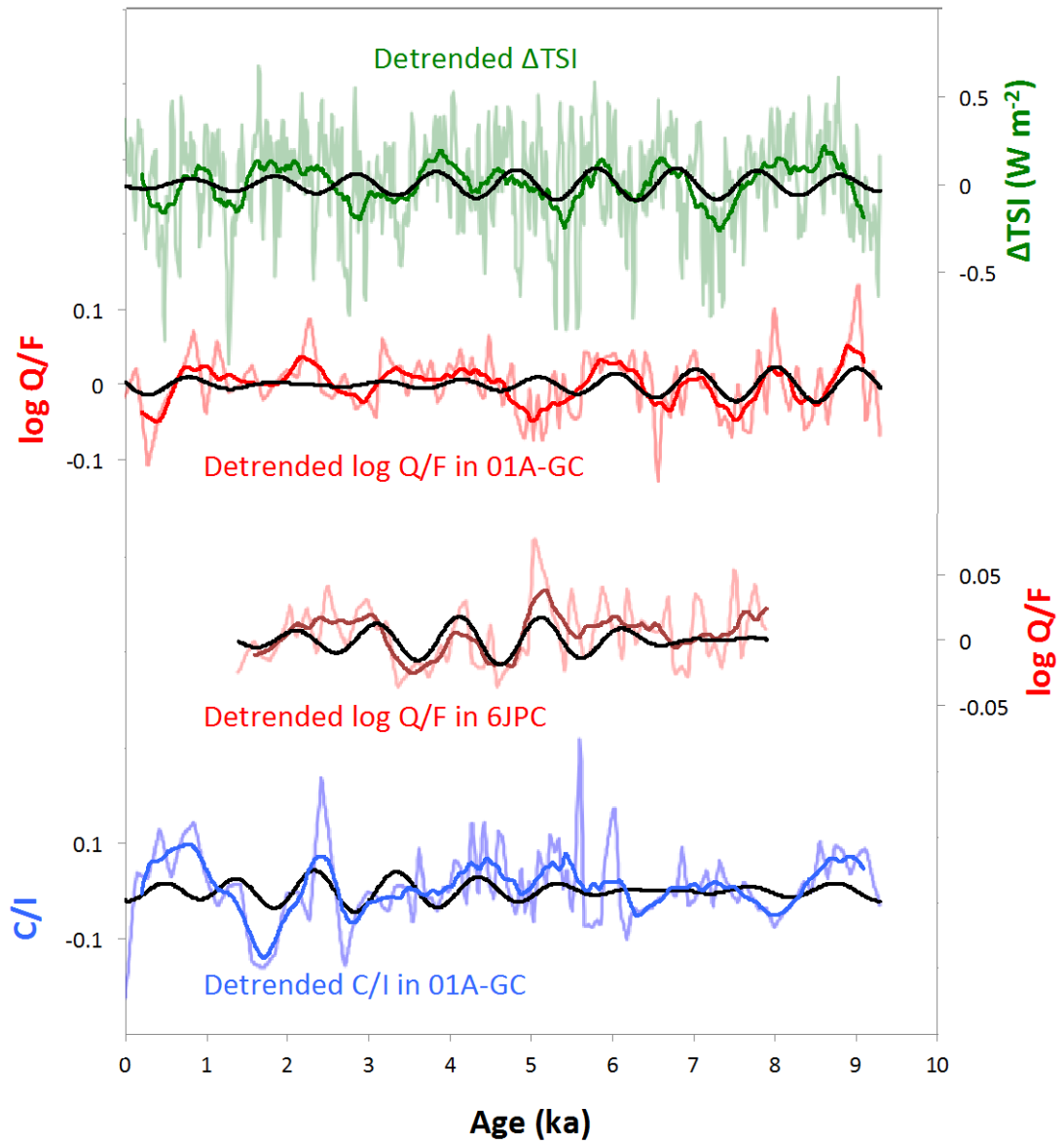
1049

1050   Fig. 7

1051

1052

1053   Fig. 8